

Platelets mediate protective neuroinflammation and promote neuronal plasticity at the site of neuronal injury

Marina Dukhinova¹, Inna Kuznetsova¹, Ekaterina Kopeykina¹, Ekaterina Veniaminova², Amanda W.Y. Yung¹, Tatyana Veremeyko¹, Natasha S. Barteneva³, Kenny Kam Wing Ho¹, Wing-Ho Yung¹, Julia Y.H. Liu¹, John Rudd^{1,4}, Sonata S.Y. Yau⁵, Tatyana Strekalova^{2,6}, and Eugene D. Ponomarev¹

Affiliations

¹School of Biomedical Sciences, Faculty of Medicine, The Chinese University of Hong Kong, Shatin, N.T., Hong Kong.

²Laboratory of Psychiatric Neurobiology, Institute of Molecular Medicine, Sechenov First Moscow State Medical University, Moscow, Russia

³Program in Cellular and Molecular Medicine, Children's Hospital Boston and Department of Pediatrics, Harvard Medical School, 200 Longwood Ave, D-239, Boston, 02115, MA, USA.

⁴Brain and Mind Institute, The Chinese University of Hong Kong, Shatin, N.T., Hong Kong.

⁵Department of Rehabilitation Sciences, The Hong Kong Polytechnic University, Hung Hom, Kowloon, Hong Kong.

⁶Department of Neuroscience, Maastricht University, Maastricht University, Maastricht, Netherlands

Corresponding author

Correspondence to: Eugene D. Ponomarev

Contributions

E.P., T.V. and N.B. conceived the study. M.D., I.K., T.V., N.B., T.S., S.Y. and E.P. designed experiments. M.D., I.K., A.Y., T.V., E.K., E.V. and E.P. conducted experiments. E.K., M.D., J.W., J.R., K.H. and W.Y. performed electrophysiology experiments. N.B. and E.P. performed flow cytometry analysis of platelet-derived microparticles. E.V., E.K., T.S. and E.P. performed and analyzed behavior experiments. M.D., I.K., T.V., E.K., S.Y., N.B., T.S. and E.P. analyzed the data. M.D., I.K., J.R., N.B., E.K., T.S. and E.P. prepared the manuscript.

Abstract

While it is accepted that inflammation within the CNS contributes to neurodegeneration during traumatic brain injury (TBI), it is not clear how inflammation is initiated in the absence of infection and whether this neuroinflammation is beneficial or detrimental. We have previously found that brain-enriched glycosphingolipids within neuronal lipid rafts (NLR) induced platelet degranulation and secretion of neurotransmitters and pro-inflammatory factors. In the present study, we compared TBI-induced inflammation and neurodegeneration in wild-type vs. *St3gal5* deficient ($ST3^{-/-}$) mice that lack major CNS-specific glycosphingolipids. After TBI, microglial activation and CNS macrophage infiltration were substantially reduced in $ST3^{-/-}$ animals. However, $ST3^{-/-}$ mice had a larger area of CNS damage with marked neuronal/axonal loss. The interaction of platelets with NLR stimulated neurite growth, increased the number of PSD95-positive dendritic spines, and intensified neuronal activity. Our study established the key role of platelet-derived factors in the regulation of neuroinflammation and neuronal plasticity after brain injury.

Subject terms: cellular neuroscience, neuroinflammation, glycobiology, platelets, neuronal plasticity, traumatic injury, microparticles;

Introduction

The central nervous system (CNS) has three distinct properties that makes it unique compared to other organs. Firstly, the CNS is highly vascularized and has a very high density of blood vessels that are closely interconnected with neuronal and glial cells composed of unified neurovascular units. Secondly, the blood is separated from neuronal cells by a complex structure known as the blood brain barrier (BBB), which is comprised of (1) continuous tight junctions between endothelial cells with suppressed transcytosis, and (2) a ring of astroglial processes that encircle the vessel and make contact with mural cells (pericytes and smooth muscle cells) that also regulate the permeability of BBB¹⁻³. Thirdly, although brain meningeal lymphatics connected with deep cervical lymph nodes were recently described⁴, the CNS parenchyma itself is devoid of mature lymphatics and lymph nodes that are central to the immune response occurs in other organs. As such, the absence of traditional lymphatics makes the vasculature the only significant interface between the brain parenchyma and the peripheral immune system.^{5,6} Despite substantial progress in understanding the role of innate immune cells in the initiation of inflammation during infection, specific signaling pathways that trigger sterile inflammation in the CNS during neurodegeneration are yet to be identified^{7,8}.

Traumatic brain injury (TBI) and its complications, such as hemorrhage, are some of the leading causes of death among young adults worldwide. TBI is associated with acute neuroinflammation, extensive neuronal damage and neurodegeneration followed by the resolution of inflammation and neuronal tissue remodeling with increased neuronal plasticity⁹. However, the pathological events that accompany TBI often overlap with the pathological processes of other neurodegenerative diseases¹⁰. For example, TBI, AD and PD are accompanied by an accumulation of aggregated proteins in the CNS (e.g. β -amyloid, synuclein), synaptic dysfunction and cognitive problems. In addition, links between

neurovascular damage/dysfunction and neurodegeneration in AD have been highlighted¹¹. Indeed, TBI is now accepted as a risk factor for AD, PD and chronic traumatic encephalopathy¹². The exact mechanisms of initiation and propagation of neuroinflammation as well as increased neuronal plasticity during the remodeling stage after TBI are not well understood and effective therapy is still lacking⁹.

Platelets (thrombocytes) play an important role in thrombosis and hemostasis when they become activated in response to vascular damage. Recent studies have demonstrated that platelets also play an important role in inflammatory diseases^{13,14}. Our studies showed that platelets actively participate in the regulation of neuroinflammation during experimental autoimmune encephalitis and multiple sclerosis (MS)¹⁵⁻¹⁷. However, the role of platelets and platelet-derived microparticles (PMPs) in CNS repair is only now emerging¹⁸. Platelets are very abundant in the blood and outnumber leukocytes almost 100-fold, and contain pro-inflammatory, vasoconstrictive and neurotransmitter molecules, which are stored in alpha- and dense granules (vesicles) and are released during activation¹⁸. Activated platelets secrete granule content via fusion of vesicles with the outer membrane in a calcium-dependent manner via a molecular mechanism similar to the process of neurotransmitter release by pre-synaptic neurons¹⁹. In addition, activated platelets intensively shed PMPs²⁰. Among the most potent vasoactive, immuno- and neuro-modulatory platelet-derived factors are serotonin (5-HT) and platelet activating factor (PAF). Platelets are the major source of 5-HT outside of CNS and are an abundant source of PAF^{21,22}.

We previously found that neuronal detergent-resistant rigid membrane domains or neuronal lipid rafts (NLR) induced massive platelet activation and degranulation¹⁷. The **brain-enriched** glycosphingolipids (gangliosides) within NLR were specifically recognized by platelets and this recognition occurred during the disruption of BBB, a classic hallmark of CNS inflammation^{16,17}. NLR were found to be localized within the endfeet of astrocytes and

on neuronal processes where NLR are particularly abundant on post-synaptic density (PSD) membranes¹⁷.

To investigate the possible role of platelets during TBI, we used *St3gal5* (*ST3^{-/-}*) mice, which lack brain-enriched gangliosides GM1, GT1b and GQ that efficiently activate platelets¹⁷. We found that after a TBI, microglia activation and leukocyte infiltration were substantially inhibited in the CNS of *ST3^{-/-}* animals when compared to wild-type (WT) controls. Surprisingly, *ST3^{-/-}* mice displayed increased damage with more pronounced neuronal loss, which was observed after resolution of the TBI-induced acute neuroinflammatory response. Here, we further establish that after TBI, platelet-derived PAF mediates microglial activation and the recruitment of peripheral monocytes, while platelet-derived 5-HT, inhibits hemorrhage and an increase in neuronal survival and plasticity. Our study also revealed that platelets induce rapid formation of dendritic spines and increased evidence of synaptic plasticity and electrophysiological outcomes. We propose that in addition to the induction of markers of neuroinflammation, platelets also increase synaptic plasticity near the site of injury and stimulate neuronal activity.

Results

***ST3^{-/-}* mice abnormally react to focal brain injury exhibiting an increased level of hemorrhage and a decreased level of neuroinflammation**

We previously found that the interaction of isolated NLR with platelets in the bloodstream caused profound platelet degranulation leading to anaphylaxis in mice¹⁷. The process of recognition of brain-enriched gangliosides GM1, GT1b and GQ was mediated through specific receptors (e.g. CD62P) on platelets, leading to the secretion of 5-HT and subsequent fragmentation of platelets into microparticles¹⁷ that are known to contain PAF²³ (**Fig. S1A**).

To investigate the role of **brain-enriched** glycolipids in the CNS during focal TBI, we used ST3^{-/-} mice that are deficient in GM3-synthase required for synthesis of major brain-enriched gangliosides²⁴ (**Fig. S1B**). Administration of NLR isolated from an ST3^{-/-} mouse brain resulted in a 3-fold lower level of anaphylaxis when compared to the same amount of NLR isolated from WT mice (**Fig. S1C**). Notably, ST3^{-/-} mice have normal CNS development, and exhibit normal phenotype in adulthood²⁴. As such, they afford a good model to study platelet-NLR interactions during TBI when platelets are in direct contact with NLR at the site of neuronal injury (**Fig. S1D**).

When we induced TBI in ST3^{-/-} mice, we found that they exhibited a 3-fold increase in hematoma size within the cortex (**Fig. 1A, B**) and a 2-fold increase in concentration of CNS hemoglobin (**Fig. 1C**), which together indicate an increased level of intracerebral bleeding. The increased bleeding in the CNS of ST3^{-/-} animals after TBI was not due to the impaired activity of platelets in these mice; platelets from ST3^{-/-} upregulated the activation marker CD62P and other activation markers in response to *in vitro* stimulation with thrombin, ADP or Collagen (**Fig. S2A-G**). ST3^{-/-} mice also have platelet counts that are comparable to WT animals and react to thrombin-induced thromboembolism *in vivo*, but they do exhibit a longer tail bleeding time (1.7-fold). Increased tail bleeding time in ST3-deficient mice could indicate possible problems with blood vessels in the periphery owing to the absence of several gangliosides in peripheral blood vessels such as GD3²⁵ (**Fig. S2H-J**). When we isolated mononuclear cells from the CNS of naive WT mice or mice with TBI, we found that ST3^{-/-} mice had lower levels (percentage and absolute numbers) of CD11b⁺CD45^{hi} peripheral macrophages/activated microglia (**Fig. 1D, E**), CD11b⁻CD45^{hi} lymphocytes (**Fig. 1D, F**), and CD4 T cells (**Fig. 1G**). Expression of pro-inflammatory cytokines TNF and IL-6 in the brain after TBI were also significantly reduced in the ST3-deficient mice (**Fig. 1H-J**) demonstrating a reduced degree of neuroinflammation in these animals. Thus, following TBI

there was more hemorrhage, but less neuroinflammation in ST3^{-/-} animals compared to the WT mice.

ST3^{-/-} mice have a low level of infiltration of peripheral macrophages and a low level of activation of CNS-resident microglia after focal TBI

We further characterized the inflammatory response in the CNS of WT compared to ST3-deficient mice by determining proportions peripheral blood-derived monocytes/macrophages as CD11b⁺Ly6C⁺ cells and resident microglia as CD11b⁺CD45^{low/int}Ly6C⁻ cells and evaluating the expression of well-known microglial cell activation markers MHC class II and CD86^{26,27}. We found that after TBI ST3^{-/-} animals had a 3-fold lower level of peripheral macrophages in the CNS (**Fig. 2A, B**) and ~2-fold lower levels of expression of activation markers MHC class II and CD86 (**Fig. 2C, D**) on microglia. This indicates a decrease in the level of infiltration of peripheral macrophages and a reduced level of microglial activation. The lower level of activation of microglia in ST3^{-/-} mice was not due to the inability of myeloid lineage cells to become activated in response to inflammatory stimuli nor the inability of platelets from ST3^{-/-} mice to activate myeloid cells. Under inflammatory conditions induced by peripheral administration of LPS, microglia from WT and ST3^{-/-} exhibited the same level of activation *in vivo* (**Fig. S3A, B**). Moreover, WT and ST3^{-/-} macrophages activated *in vitro* with either IFN- γ or lipopolysaccharide (LPS) or co-incubated with autologous platelets exhibited a similar level of expression of activation markers and were both capable of providing a normal inflammatory response (**Fig. S3C, D**). Thus, we conclude that ST3^{-/-} mice respond to injury with a lower level of neuroinflammation, and more hemorrhage after TBI, due to impaired platelet-NLR interactions in the CNS.

After TBI, platelets become fragmented into microparticles upon interaction with NLR in WT mice and accumulate in the CNS of ST3^{-/-} mice

We next investigated the presence of CD41⁺ platelets in the CNS and their co-localization with NLR after TBI. Fluorescently labelled *Cholera Toxin B* subunit (CTB) is known to bind with GM1 ganglioside was used as a NLR marker. We found the CTB-labeled NLRs in the CNS of WT and ST3^{-/-} mice, but the NLR sites were more evident in WT mice (**Fig. 2E, F**). This is consistent with the fact that ST3^{-/-} mice still have CNS populations that express gangliosides (**Fig. S1B**) that are able to bind to CTB^{28,29}. After TBI, in the CNS of both WT and ST3^{-/-}, animal platelets were detected in close proximity to CTB-labeled NLR (**Fig. 2E, F**). Further analysis revealed that after TBI in WT mice, platelets become fragmented into microparticles that express the pro-inflammatory mediator PAF on their surface (**Supplementary Results, Part 1, Fig. S4**). However, in the CNS of ST3^{-/-} mice, more platelets were found close to blood vessels as determined by immunofluorescence (**Fig. 2E, F**). After TBI, ST3-deficient mice exhibit lower levels of microglial activation and higher level of fibrinogen depositions in the CNS (**Fig. S5A, B, D**). In naive ST3^{-/-} animals, the populations of BBB associated mural cells (pericytes and smooth muscle cells) appeared to be normal (**Fig. S5C, E, F**) and the uninjured mice exhibited an intact BBB as determined by fibrinogen deposition (**Fig. S5A, B**) and i.v. injection of Evans Blue dye (not shown). Thus, the interaction of platelets with NLR resulted in their degranulation and fragmentation in WT mice and accumulation in the CNS of ST3^{-/-} animals on day 1 after TBI.

Injection of NLR at the site of injury enhanced neuroinflammation after TBI

To investigate whether the interaction of platelets with NLR enhances neuroinflammation and results in a decreased in hemorrhage in WT mice, we decided to attempt to rescue the phenotype of ST3^{-/-} by administrating WT NLR. Since the interaction of platelets with NLR

takes place locally and within minutes¹⁷, we decided to inject PBS or NLR derived from WT or ST3^{-/-} mice, as a weak (not ganglioside specific) platelet activator at the site of TBI (**Fig. 3A**). Administration of WT NLR but not ST3^{-/-} NLR substantially increased the percentage of CD11b⁺CD45^{hi} peripheral macrophages/activated microglia in the CNS of WT and ST3^{-/-} mice (**Fig. 3B**). Thus, the interaction of platelets with WT NLR at the site of TBI resulted in a dramatic increase in neuroinflammation.

Platelet-derived PAF and 5-HT strictly control the extent of neuroinflammation and hemorrhage after TBI

We previously found that upon interaction with NLR, platelets secrete a high level of 5-HT and produce large numbers of microparticles that contain PAF on their surface^{16,17} (**Fig. S4**), and both PAF and 5-HT were shown to be potent pro-inflammatory agents¹⁶. PAF receptors (PAFR) are highly expressed on microglia and macrophages, as well as neurons, and they play an important role in neuroinflammation, neurodegeneration and pain³⁰⁻³². Therefore, we tested the role of PAF by injecting a PAFR antagonist to the site of TBI as we did for NLR (**Fig. 3A**). We found that a PAFR antagonist significantly reduced the level of neuroinflammation in WT mice to the level comparable to ST3^{-/-} animals as determined by the extent of peripheral macrophage infiltration (**Fig. 3C**) and microglia activation (**Fig. 3D**).

In a similar way to PAF, we investigated the role of 5-HT in the development of neuroinflammation. Surprisingly, an injection of a blocking anti-5-HT serum at the site of TBI increased the level of peripheral macrophage infiltration and thus extended the neuroinflammation (**Fig. 3E**). In addition, we systemically inhibited 5-HT synthesis with p-chlorophenylalanine (PCA). It is established that PCA effectively stops 5-HT synthesis³³ and reduces 5-HT level in thrombocytes. Blocking of 5-HT synthesis yielded results similar to the administration of anti-5-HT serum at the site of TBI (**Fig. 3F**). To further investigate the

regulatory role of 5-HT in our model, we injected 5HT at the site of TBI which decreased the level of periphery macrophage infiltration in both WT and ST3^{-/-} mice, confirming the anti-inflammatory properties of 5-HT during TBI (**Fig. S6A**).

As other cell populations might contribute to the total level of 5-HT and PAF in the CNS after TBI besides platelets, we performed adoptive transfer experiments (**Fig. S6B, C**) where only platelets were unable to produce PAF (**Fig. S6D**) or 5HT (**Fig. S6E**) in response to NLR. To perform these experiments we used a recently described mouse strain by crossing the PF4-Cre mice with the Rosa26-DTR transgenic mouse³⁴. Wild-type mice do not express receptors for diphtheria toxin (DTx), but PF4-CreXRosa26-DTR mice express diphtheria toxin receptors (DTR) in platelets alone and allowed us to selectively deplete platelets following the administration of DTx (**Fig. S6C**). We confirmed the principal role of platelet-derived 5HT and PAF by transferring platelets lacking in 5-HT or PAF (**Fig. S6B**) to recipient mice that had been platelet depleted (**Fig. S6C**). These experiments clearly demonstrated that inhibition of platelet-derived phospholipid mediators, such as PAF, decreased neuroinflammation, while inhibition of platelet-derived 5-HT increased inflammation after TBI (**Fig. S6F**). This indicated that platelets produce pro- and anti-inflammatory factors that tightly control the extent of neuroinflammation after TBI.

Injection of NLR or 5HT at the site of injury decreased hemorrhage

As ST3^{-/-} mice exhibited reduced levels of neuroinflammation and increased hemorrhage (**Fig.1**), we hypothesized that neuroinflammation may play a protective role by decreasing hemorrhage and might restrict the area of damage. We found that WT NLR increased neuroinflammation (**Fig. 3A-B**), and an injection of WT NLR (but not ST3^{-/-} NLR) at the site of TBI of ST3^{-/-} also reduced hemorrhage 2-fold to a level comparable to that of WT animals (**Fig. 3G**). When we analyzed what platelet-derived factors decrease intracerebral

hemorrhage in ST3^{-/-} animals, we performed an initial screening by the administration of specific agonist/antagonists for platelet-derived factors including 5-HT for its known vasoconstrictive properties³⁵. Indeed, an injection of 5-HT at the site of TBI reduced hemorrhage 2-fold in ST3^{-/-} mice to the level of WT animals (**Fig. 3H**), while an injection of PAFR antagonists had no effect on the extent of hemorrhage (not shown). Thus, the relationship between inflammation and hemorrhage appear to be complex. We concluded that the interaction of platelets with NLR increased inflammation and at the same time resulted in the release of platelet-derived 5-HT, which ultimately decreased hemorrhage and restricted infiltration of peripheral macrophages.

ST3^{-/-} mice display a large area of damage with astroglial scars and neuronal loss

Based on the previous findings we hypothesized that platelet-mediated neuroinflammation has a protective role during the later stages of TBI by restricting the size of the damage and promoting CNS repair near the trauma site. To test this, we investigated the area of brain damage 3 days after TBI when neuroinflammation was mostly resolved (**Fig. 1D**). We found that starting from day 4, GFAP^{+ve} astroglial cells became evident at the site of injury in WT and ST3^{-/-} animals (not shown), and that by day 7 the area of the astroglial scar was 2.5-fold larger in the ST3^{-/-} mice (**Fig. 4A-C**). The scar area in ST3^{-/-} mice was also characterized by a marked increase in neuronal loss when compared to WT mice as determined by β 3-tubulin staining, which detects the presence of neuronal bodies and neurites, and Cresyl Violet staining, which marks neuronal bodies (**Fig. 4A, B, D**). Thus, the interaction of platelets with NLR resulted in a decreased area of neuronal loss with reduced astroglial scar formation.

ST3-deficient mice display impairments in cognitive and motor functions after TBI compared to WT animals

In order to study behavioral effect of the ST3^{-/-} mutation following TBI, behavioral tests were performed to examine gross motor function, general locomotion, hippocampus-dependent plasticity, social interaction, novelty exploration, as well as impulsivity- and anxiety-like behaviors. The performance of uninjured ST3^{-/-} mice in the open field, novel cage, Y-maze, and in acquisition of new object recognition task was unaltered compared to WT mice (**Supplementary Results, Part 2, Fig. S7**). The uninjured ST3^{-/-} mice displayed small, but notable, impairment of motor function in the wire and rotarod tests (**Supplementary Results, Part 2, Fig. S7; Fig. 4I, Unmanipulated mice**). However, improved scores were recorded for the ST3^{-/-} mice in the Barnes maze test of measure spatial learning and memory (**Fig. 4E, G**). After TBI, ST3^{-/-} exhibited poorer performance in the Barnes maze (Fig. 4F, H) and rotarod (**Fig. 4I**) tests when compared with WT animals. Thus, TBI resulted in significant decrease in cognitive and motor functions in ST3-deficient animals.

Direct interaction of platelets with neurons leads to the stimulation of axonal growth, increase in neuronal cell density, and induction of expression of neuronal early response and synaptic plasticity genes

To investigate whether platelets directly affect neuronal functions after TBI, we co-incubated cortical neurons with platelets. Platelets directly interacted with neurons making cell-cell contacts with neuronal cell bodies and processes (**Fig. 5A**). We found that a co-incubation of platelets with neuronal cells for 3-6 days stimulated the growth of neurites (**Fig. 5B, C**) and substantially increased neuronal cell density (**Fig 5B, D**). It is established that 5-HT could serve as a neurotrophic factor that stimulates axonal growth³⁶. Since 5-HT is abundantly secreted by platelets stimulated by NLR^{16,17}, we investigated the role of platelet-derived 5-HT in the stimulation of axonal growth. We found that the addition of anti-5-HT serum to platelet-neuronal co-incubation cultures completely inhibited platelet-mediated induction

neurite growth (**Fig. S8A** and **Fig. 5E**) and increased neuronal cell density (**Fig. S8A, B**). To investigate the effect of platelets on neurons at a molecular level, we performed selective quantitative profiling of early response genes and genes responsible for synaptic plasticity following co-incubation of neurons with platelets. We found that platelets stimulated the early response genes *c-Fos*, *c-Jun*, *Arc* and *Egr-1* that are involved in increased neuronal activity³⁷ (**Fig. 5F**). Platelets also induced the synaptic plasticity genes *Synapsin-1 α* , *PSD95*, *BDNF* and its receptor *TrkB*³⁸ (**Fig. 5F**). When we investigated the role of platelet-derived 5-HT in the upregulation of *Arc*, *Synapsin-1 α* , *PSD95*, *BDNF* and *TrkB*, we found that the enhanced expression of all these genes by platelets was blocked by anti-5-HT serum (**Fig. S8C**). Thus, we determined that platelets directly interacted with neurons and platelet-derived 5-HT as they directly supported neuronal plasticity and stimulation of neuronal functions.

Platelets directly interact with lipid raft-rich neuronal processes, induce formation of PSD95-positive dendritic spines, and stimulate electrical activity of neurons

As platelets induced the expression of a number of synaptic genes in neurons, we investigated whether platelets could directly interact with neuronal processes and promote structural changes associated with enhanced synaptic plasticity. We found that platelets did interact with neuronal process enriched with GM1⁺ NLR (**Fig. 6A**). By using high resolution scanning electron microscopy (SEM), we found the presence of contacts of platelets with neuronal processes (**Fig. 6B**). Further analysis of SEM images revealed that platelets stimulated the formation of mature dendritic spines³⁹ as early as 8-16h after co-incubation (**Fig. 6C, D**). One of the well-known markers that is associated with the NLR-rich PSD membranes of dendritic spines is PSD95⁴⁰. PSD95 is also expressed in formed synapses, but in this case PSD95 is co-localized with Synapsin-1⁴¹. We found that platelets stimulated increased levels of expression of PSD95 mRNA (**Fig. 5F**) and protein levels as determined

by immunofluorescence and Western blot analyses (**Fig. 6E, F**). Co-localization analysis also demonstrated that PSD95 expression was upregulated on dendritic spines when PSD95 was not co-localized with Synapsin-1 (**Fig. S9**).

Upregulation of early response/synaptic genes may indicate an increase in functional activity of neurons. Indeed, platelets increased spontaneous electrical activity of cultured neurons after 24h of co-incubation with platelets as determined by the number of high amplitude spikes detected by using a multielectrode array system on a group of neurons and by patch clamp analysis of individual neurons (**Fig. 6G, H**). Taken together, our data demonstrated that platelets directly interacted with neurons including their processes, induced formation of PSD95-positive dendritic spines, and stimulated electrophysiological activity of neurons.

Expressions of synaptic markers Synapsin-1 and PSD95 are dramatically reduced in ST3^{-/-} mice after TBI

We evaluated the expression of Synapsin-1 and PSD95 markers *in vivo* in the CNS after TBI. On days 3-7 after focal TBI, the expression of mRNA for Synapsin-1 α and PSD95 was reduced 3-fold in WT animals. However, in ST3^{-/-} mice, the decrease in Synapsin-1 α and PSD95 mRNA and protein was evident as early as day 2, and the expression of both markers was more substantially decreased in ST3-deficient mice by day 3-4 (**Fig. 7A-C**). We further characterized the expression of PSD95 and Synapsin-1 protein levels at the site of TBI by immunofluorescence. In normal unmanipulated WT and ST3^{-/-} mice, the expression of Synapsin-1 exhibited a perinuclear pattern of localization in neuronal bodies as indicated by arrows (**Fig. 7D**) in addition to the expression of Synapsin-1 in the periphery of the cells (**Fig. 7D**). On d7 after TBI in WT and ST3^{-/-} mice, the perinuclear localization of Synapsin-1 was undetectable and there was a small change in the total expression of the total level of

Synapsin-1 (**Fig. 7D-F**). However, the peripheral expression of Synapsin-1 was dramatically increased in WT animals, but not ST3^{-/-} mice (**Fig. 7D-F**), after TBI. Expression of total PSD95 was also increased in WT, but not in ST3^{-/-} mice (**Fig. 7D-F**), with a more dramatic increase in PSD95 expression on dendritic spines (**Fig. 7G, H**). Notably, the expression of PSD95 on dendritic spines increased 8-fold in WT mice (**Fig. 7G**), while it decreased 8-fold in ST3^{-/-} animals (**Fig. 7H**), demonstrating a dramatic difference between WT vs. ST3^{-/-} animals. Thus, in contrast to WT mice, expressions of PSD95 and Synapsin-1 on neuronal processes were dramatically reduced in ST3^{-/-} mice after TBI.

Platelets stimulate expression of Synapsin-1 and PSD95, induce expression of endogenous BDNF and its TrkB receptors, and promote neuronal survival in WT but not ST3^{-/-} organotypic brain slice cultures

To further investigate the mechanism of upregulation of PSD95 and Synapsin-1 after TBI in WT mice, we used organotypic brain slice cultures from adult, 3-4-week-old mice that contain all CNS resident cells and serve as a good model for TBI without the influence of blood-derived cells⁴². This brain slice model of TBI was characterized by neuronal loss with microglial activation (**Fig. S10, BS Only**). We confirmed that platelets induced *Synapsin-1* and *PSD95* expressions in WT (but not ST3^{-/-}) brain slices as revealed by altered mRNA (**Fig. 8A, B**) and protein levels (**Fig. 8C-E**). In addition, platelets induced mRNA for *BDNF* and *TrkB* receptors in WT, but not in ST3^{-/-} brain slices (**Fig. 8A, B**), and significantly increased neuronal survival in WT brain slices (**Supplementary Results, Part 1, Fig. S11B-D**). At the same time, the addition of platelets did not increase microglial activation in brain slices and even had trend for decrease in microglia activation in WT, but not ST3-deficient brain slices (**Fig. S10, BS + Platelets**). Thus, these data further supported our hypothesis that

platelet-NLR interactions resulted in induction of expression of BDNF, TrkB, Synapsin-1, and PSD95.

ST3-deficient mice have higher density of dendritic spines on neurons and higher level of spontaneous electric activity in brain slices, which is not modulated by electromagnetic stimulation of addition of platelets

We further compared the number of dendritic spines and neuronal electric activity in WT and ST3-deficient brain slices. Using *Golgi* staining, we found that ST3^{-/-} mice have higher levels of dendritic spines at the baseline level when compared to WT brain slices. The addition of platelets did not influence number of dendritic spines in ST3^{-/-} animals, but resulted in increase in dendritic spine density in WT brain slices (**Fig. 12A, B**). In addition, ST3-deficient mice have higher level of baseline neuronal electric activity in brain slices when compared to WT brain slices (**Fig. S12C, *Brian Slices Only, Baseline***). Electromagnetic stimulation (**Fig. S12C, *Brian Slices Only, Baseline***) or addition of platelets (**Fig. S12C, *Brian Slices + Platelets, Baseline***) or both (**Fig. S12C, *Brian Slices + Platelets, Stimulated***) increased neuronal electric activity in WT, but not in ST3^{-/-} brain slices. Thus, ST3^{-/-} mice have higher number of dendritic spines and higher level of electric activity, which was not influenced by electromagnetic stimulation or addition of platelets.

Addition of platelets to wild-type brain slices resulted in upregulation of multiple genes involved in pro-inflammatory, neurotrophin, synaptic, and oxidative phosphorylation pathways

As platelets induced increase in dendritic spine density in WT brain slices, we performed whole transcriptome RNA-seq analysis of differential gene expression in brain slices incubated alone or co-incubated with platelets. We found that addition of platelets resulted in

upregulation of pro-inflammatory genes (e.g. *TNF*, *IL-1*), neuronal early response neuronal genes (e.g. *ARC*, *EGR1*), and mitochondrial genes (e.g. *MT-CYTB*, *MT-ND*) (**Fig. S12D**). Analysis of the pathways involved demonstrated up-regulation of those pathways involved in synaptic function, neurotrophin signaling pathway, TNF signaling, antigen presentation, and oxidative phosphorylation (**Fig. S12E**). Among the downregulated pathways were the protein digestions and adsorption, immunodeficiency and glycolysis (**Fig. S12F**). Thus, large profiling experiments confirmed upregulation of multiple genes involved in inflammation, neuronal early response and synaptic plasticity genes.

Platelet-derived 5-HT stimulated expression of PSD95 and Synapsin-1 through the BDNF-TrkB pathway

To further understand the mechanisms of induction of synaptic plasticity genes BDNF, TrkB, Synapsin-1, and PSD95 by platelets in brain slices, we added blocking anti-5HT serum during co-incubation of platelets with brain slices. We found that anti-5-HT serum completely blocked platelet-induced expression of mRNA for all these molecules (**Fig. 8F**). The addition of blocking anti-BDNF antibodies to same co-incubated cells had a very similar effect (**Fig. S11A**). Given the fact that mouse platelets do not produce BDNF⁴³ while 5-HT induces endogenous BDNF⁴⁴ synthesis leading to formation of dendritic spines⁴⁵, we proposed a model of interaction of platelets with NLR located on neuronal processes (**Fig. 8G**). Thus, based on our data, we have established a model whereby the interaction of platelets with the NLR promotes neuronal plasticity via secretion of 5HT, that in turn, induces BDNF and TrkB receptors on dendritic spines (**Fig. 8G**).

Discussion

In the current study, we demonstrated that platelets play an important role in the regulation of neuroinflammation and neuronal plasticity at the trauma site. Many types of neurologic diseases such as TBI and stroke are accompanied by neuroinflammation followed by increased neuronal plasticity near the site of injury, but the exact mechanisms of these phenomena are not known⁴⁶. By performing systemic analysis of neuroinflammation and neuronal functions in mice that lack brain-enriched gangliosides, we demonstrated a key role for platelets in the control of neuroinflammation and the induction of neuronal plasticity.

The role of platelets and platelet-derived factors in regulating neuroinflammation and neurogenesis/repair during AD, PD, stroke and MS has been proposed^{15,16,18,47}. However, our study establishes an important link between CNS tissue damage and platelet activation: the presence of specific glycolipid structures are directly recognized by platelets when BBB is disrupted¹⁷. This study further supports our hypothesis that platelets serve as primary “alarm danger signals” of neurovascular damage in the CNS^{16,17}.

The role of major brain glycolipids in neurologic disorders still not well understood. In this study, we used deficient for *st3gal5* gene, which encode enzyme required for glycosylation of major brain gangliosides. Mutations in this gene in humans result in number neuropsychiatric diseases that include epilepsy and cognitive disabilities⁴⁸⁻⁵¹. Earlier reports suggested that ST3-deficient mice did not show substantial phenotype²⁴, but phenotype of these mice was not investigated in details. Our study demonstrated that ST3-deficient mice exhibit higher level of spontaneous electric activity and higher density of dendritic spines, which may indicate why humans with such mutations are more prone to epilepsy associated with increased electric activity of group of neurons or neuropsychiatric abnormalities

associated with increased number of synaptic connections. On the other hand, we showed that ST3-deficient mice have some motor problems, which are accentuated after injury. Moreover, ST3^{-/-} mice displayed serious cognitive problems after brain focal injury, while this type of mild injury had practically no effect on WT mice. This finding may explain why humans with mutation in *st3gal5* gene are more prone to development of neuropsychiatric symptoms after minor brain trauma, which are especially common in childhood.

Since major brain gangliosides are localized in NLR close to BBB structure they play an important role by interacting with platelets and serve as “danger signals” from immune cells and neurons during injury^{16,17}. The role of the blood vessel and BBB pathology in neurodegenerative diseases has received more attention recently. In AD, ApoE gene was found to be associated with increased risk of the disease and ApoE-deficient mice have compromised BBB^{52,53}.

Upon the recognition of NLR, platelets immediately degranulate with subsequent budding into microparticles producing a number of pro-inflammatory mediators (e.g. PAF) and neurotransmitters (e.g. 5-HT)^{16,17}. Our previous studies indicate that interaction of platelets with neuronal lipid rafts occurs within minutes leading to secretion of platelet-derived factors¹⁷. We propose that the factors that platelets secrete during early stage of TBI affect inflammation and outcome of the injury. It is known that 5-HT is promptly released by platelets from dense granules¹⁶, while PAF is mostly expressed on the surface of platelet-derived microparticles²³ that play a pro-inflammatory role¹³. In addition to PAF, 5-HT was also shown to be pro-inflammatory¹⁶, but recently it was demonstrated that 5-HT could induce alternative M2 macrophage/microglia activation to play a regulatory role during neuroinflammation and promote tissue repair^{54,55}.

Based on this study, we propose dynamic platelet–neuron synapse-like structures form after TBI when the BBB is disrupted. Formation of platelet–neuron contacts resulted in the

release of 5-HT by platelets that induced expression of endogenous BDNF and TrkB receptors in NLR-rich PSD membranes⁵⁶ leading to enhanced neuronal plasticity and upregulation of PSD95 inside of the newly formed dendritic spines (**Fig. 8G**). In contrast to humans, mouse platelets do not produce BDNF, but they produce a high level of 5-HT that stimulates endogenous BDNF in neurons^{43,44}. Serotonin 5-HTR_{2A} receptors are located in NLR-rich PSD membranes and signalling through this receptor causes dendritic spine enlargement⁵⁷. It was recently shown that endogenous rather than exogenous BDNF increased synaptic plasticity⁴⁵. Our experiments show that platelet-derived 5-HT upregulates BDNF in neurons, which, in turn stimulated synaptic plasticity through altered gene expression. Platelets also stimulated the spontaneous electrophysiological activity of neurons that could also enhance their synaptic plasticity⁵⁸.

Taken together, our study introduces a new concept that platelets directly recognize CNS injury and produce a number of factors that induce neuroinflammation, decrease hemorrhage and stimulate neuronal functions and synaptic plasticity. We believe that our findings have applications for the future therapy of TBI and other neurodegenerative diseases by targeting platelet-NLR interactions.

Methods

Mice

Colonies of B6 (C57BL/6) and *St3gal5* (ST3^{-/-}) deficient mice used in our previous studies¹⁷ were maintained at the Laboratory Animal Service Centre (LASEC) at the Chinese University of Hong Kong (CUHK). B6.Gt(ROSA)26Sor^{tm1(HBEGF)Awai}/J and B6.Tg(Pf4-icre)Q3Rsko/J mouse strains were purchased from Jackson Laboratories and maintained in LASEC. All animal protocols were approved by the Government of Hong Kong Department

and the Chinese University of Hong Kong Animal Experimentation Ethics Committee. For experiments that involved pain and distress, the appropriate anesthetic drugs (isoflurane) were used. Euthanasia was performed using carbon dioxide. To activate microglia *in vivo*, B6 or ST3^{-/-} were injected i.p. with LPS (1 mg/kg) for 4 days as previously reported⁵⁹.

Focal traumatic brain injury model

8-12-week-old female animals were used in the experiments. To induce focal TBI, a 25g needle was inserted 1mm deep from the top of the dura into the left or right hemisphere of the prefrontal cortex as described previously⁶⁰. The extent of the intracerebral hemorrhage was assessed by measuring the intracerebral hematoma and by spectrophotometric analysis of the CNS hemoglobin concentration as described⁶¹. In several experiments, 20 μ l of PBS alone, or 20 μ l of PBS with a suspension of NLR (5 μ g phospholipids/ml), dissolved 5-HT (1 mg/ml), or PAFR antagonist (WEB2076; 1 mg/ml), or anti-5-HT (4 μ g/ml), or control serum (4 μ g/ml) was injected at the site of injury through the 25g needle via a syringe. To inhibit PAF synthesis in platelets, the irreversible inhibitor of PLA2 (methyl-arachinodoyl-fluorophosphonate; MAFP) was injected daily i.p. for 3 days at 5 mg/kg. To inhibit peripheral serotonin synthesis p-chlorophenylalanine (PCA) was injected daily i.p for 3 days at 200 mg/kg as described previously³³. For all experiments, several concentrations of inhibitors or serums were used, according to the relevant literature and optimal dosages were determined as being the most effective in the absence of obvious adverse side effects. Conditional platelet depletion and subsequent reconstitution was performed using a modified model as recently described³⁴. Briefly, PF4-DTR tg mice that express receptors for DTx in platelets were obtained by crossing B6-Gt(ROSA)26Sor^{tm1(HBEGF)Awai}/J and B6-Tg(Pf4-icre)Q3Rsko/J. To deplete platelets PF4-DTR tg mice were injected i.p with 400ng/animal DTx on day 0, 2 and 4. Platelet numbers in

the peripheral blood were monitored on d7 using a hemocytometer. On day 7 PF4-DTR tg mice with depleted platelets were reconstituted, with platelets from donor B6 mice that were pre-treated with PBS (Control), MAFFP, or PCA as described above. For reconstitution, platelets from donor mice were washed, re-suspended in PBS and injected i.v. $5-7 \times 10^8$ /mouse in 200 μ l. TBI was induced 2h after platelet reconstitution and inflammation and hemorrhage was analyzed 24 h post-TBI.

Biochemical isolation of neuronal lipid rafts (NLR)

NLR were isolated by the homogenisation of the mouse brain tissue isolated from WT or ST3^{-/-} animals in PBS with 0.5% Triton X-100 and then washed in PBS as described¹⁷. The amount of NLR was quantified using a kit for the measurement of the concentration of phospholipids (Wako Chemicals) at a concentration of 5 μ g of phospholipids per ml¹⁷.

Induction of anaphylaxis and thrombin-induced thromboembolism

The mice were injected i.v. with a previously determined dose of WT or ST3^{-/-} NLR (5 μ g phospholipids/ml; see above) or thrombin (1000U/kg) and analyzed for anaphylactic clinical scores or respiratory arrest as described earlier¹⁷. The clinical scores for anaphylaxis were assessed as follows: 1) restless behavior; 2) loss of consciousness; 3) dyspnea; 4) death.

Cell isolation and cultures

Mouse primary cortical neurons were isolated from prenatal d17-18 embryos as described²⁶. Brain slice organotypic cultures (thickness 500 μ) from 21-28-day old B6 or ST3^{-/-} mice were performed as described⁴⁵. Neuronal cells were cultured using a neurobasal medium with B27 supplement, 0.5% glutamate and 1% penicillin/streptomycin. Washed mouse platelets were isolated from platelet-rich plasma as described¹⁶ and were added to neuronal cultures at the

cellular ratio neuron-platelet of 1:10. We titrated number of added platelets to cultured neurons or brain slices and examined kinetics of expression of several synaptic plasticity neuronal genes (e.g. *PSD95*, *Syn-1*). We found that at high numbers of platelets (>1:5), there is upregulation of neuronal genes as early as 4-8h after co-incubation. However, at higher platelet numbers (more than 1 to 5 of neuron to platelet ratio), there was detrimental effect of added platelets that affected neuronal viability, which was significantly decreased after 48h after co-incubation. Therefore, we used lower (optimal) number of platelets (1:10). When we used this optimal number of platelets, we found that upregulation of neuronal genes was still detected after 8h, but the level of expression reached maximum after 24h and remained stably high for 72h. The level of expression of examined neuronal genes was comparable at 24h and 48h hours of co-incubation. At optimal platelet number (1:10), we did not see any detrimental effect on neuronal viability. Based on these data we examined expression of neuronal genes 24h or 48h of co-incubation with platelets, which were added at ratio of 1 to 10.

To isolate mononuclear cells from the CNS, the mice were perfused with PBS, the brains were dissected, homogenized, and mononuclear cells were isolated using a 40%/70% Percoll gradient as described previously^{26,62}. Isolation of mononuclear cells from cultured brain slices was performed using 40%/70% Percoll gradient similar to the isolation of the cells from CNS.

Bone marrow derived macrophages (BMDMs) were obtained from the bone marrow of 6-8 week-old B6 or ST3^{-/-} mice and grown in M-CSF (10 ng/ml) for five days as described in our previous experiments²⁶. BMDMs were cultured alone or co-incubated with syngenic platelets at the macrophage-platelet ratio of 1:5, 1:10, and 1:20 or stimulated with LPS (200 ng/ml) and IFN- γ (100 ng/ml), or GM-CSF (50 ng/ml) and IFN- γ (100 ng/ml) for 24h as described earlier^{15,26}.

A mouse neuronal cell line (neuroblastoma NIE115 cells) was purchased from ATCC and was maintained and used in our experiments as described earlier⁶³. Saponin was used at concentration 1-4 ng/ml.

Flow cytometry

CNS mononuclear cells were stained with anti- CD11b, Ly6C, CD45, CD86 and MHC class II antibodies and analyzed by 5-colour flow cytometry as described earlier^{16,17,26,62}. Absolute number of the cells was calculated by multiplying total number of CNS mononuclear cells determined by hemocytometer by the percentage of the cell populations determined by flow cytometry. Mouse platelets and platelet derived microparticles (PMPs) were stained with anti- CD61, anti-CD41, and anti-PAF antibodies and analyzed by flow cytometry^{16,17}. Platelet and macrophage activation were assessed as described previously^{15,17}. Briefly, platelets were activated with various concentrations of thrombin (0.1-1 U/ml), ADP (2-20 μ M), or Collagen (5-50 μ g) and stained for CD61, CD41, CD62P, or active form of β 3 integrin (JON/A mAbs), or CD31, or LAMP-1. CD61⁺CD41⁺ gated platelets were analyzed for the expression of activation markers using three-color flow cytometry. BMDMs were stained for CD11b, F4/80, CD86 and MHC class II and CD11b⁺F4/80⁺ gated macrophages were analyzed for MHC class II and CD86 by four-color cytometry. All samples were analyzed using a BD

LSRFortessa Flow Cytometer and a BD FACSAria Fusion Cytometer (both from BD Biosciences).

Western blot

Western blot analysis for PSD95 and Syn-1 was performed in a similar manner to that described in our earlier studies²⁶. Anti-PSD95 and anti-Syn-1 antibodies were purchased from Cell Signaling.

Microscopy and imaging

The normal mice or mice with TBI were perfused with PBS, and then 1% of paraformaldehyde in PBS. The brains were dissected and fixed in 1% of paraformaldehyde in PBS for 24h, and then dehydrated in 30% sucrose in PBS for 3-5 days. 10 μ -thick frozen sections were prepared and stained for NLR with CTB-FITC, or antibodies for GFAP, or β 3-tubulin, or PSD95, or Synapsin-1, or CD41, fibrinogen, lectin, Iba1, PDGFR, actin combined with the secondary antibodies conjugated with AF594. Brain sections were also stained with cresyl violet (Sigma) to detect the neuronal bodies. Golgi staining was performed using Bioenno-Tech Slice Golgi kit (cat# 003760) according to manufacturer's instructions. The following imaging systems were used in our experiments: Carl Zeiss Axiophot-2 Microscope Integrated Biological Imaging System; Olympus IX83 Inverted Microscope with ZDC; confocal system with inverted microscope Olympus FV1000; confocal system with motorized stage and SIM scanner Olympus FV1200.

\

Scanning electron microscopy

Mouse cortical neurons were cultured on poly-L-lysine coated coverslips for two weeks and then co-incubated with syngenic washed platelets (ratio 1:10) for 0.5-16 hours. Following this, the cells on coverslips were washed, fixed with 2.5% glutaraldehyde, then with 2% osmium tetroxide, dehydrated in ethyl alcohol and placed in a LADD Critical Point Dryer as described¹⁶. Samples were mounted on specimen stubs and coated with gold-palladium using an Edwards Sputter Coater and examined using a Hitachi SU8010 Scanning Microscope.

Electrophysiology

The electrophysiological activity of 2-3-week-old cultured single neurons, or 3-4 week old acute brain slices alone for 24h or those co-incubated with platelets or for 24h or subjected to electromagnetic stimulation were assessed by a multielectrode array (MEA) or patch-clamp system as previously described⁶⁴. Patch clamp from individual neurons and measuring of field excitatory postsynaptic potential (fEPSP) experiments were performed using Axon and Hecla setups similarly as described⁶⁵.

Real time PCR and RNA-seq analysis

For RNA isolation from brain tissues or cultured cells, the samples were homogenized and lysed using QIAzol Lysis Reagent (Qiagen) as described earlier in our studies^{26,62}. RNA purification with DNase digestion was performed using a miRNeasy Mini Kit from Qiagen. Real-time RT PCR was performed using ABI ViiA 7 and ABI QuantStudio 7 (QS7) Flex Systems. Whole transcriptome RNA-seq analysis was performed as described in Supplementary Methods (**Supplementary Materials**).

Analysis of PAF and 5HT production by platelets

PAF and 5HT concentrations were measured using liquid chromatography combined with mass spectrometry (LC/MS) using Agilent 6460 Triple Quadrupole LC/MS System. Platelets were freshly isolated from PBS-, MAFP- or PCA-treated animals and incubated with biochemically isolated NLR or with PBS for 20 min and centrifuged at high speed (14,000 rpm) similarly as described¹⁷. The supernatant was mixed with acetonitrile (1:1 v/v) for further analysis of LC/MS system. 5HT (precursor ion 177 m/z, product ion 160 m/z) and PAF (precursor ion 524 m/z, product ion 184 m/z) were analyzed using positively charged C18 column. Quantitative analysis was performed using Agilent MassHunter software. Purified 5HT and PAF were used as standards (both from Sigma).

Behavior tests

Open field, motor functions tests (wire test, pole test and rotarod test), elevated plus maze, Y-maze spontaneous alternations test, Barnes maze, new object recognition paradigm, food pellet displacement tube test and social interaction test were performed as described in details in Supplementary Methods (Supplementary Materials).

Statistical Analysis

For experiments with multiple time-points we used 3-4 mice per group and repeated experiment at least two times. For experiments with single time-point we started with pilot experiment with 2-3 mice, then we repeated it using larger groups of 4-5 mice. Usually we repeated experiment with larger group two times. If we observed statistical significance

between experimental groups in one experiment, we demonstrated one representative experiment. If we saw difference between groups substantial but not significant, we combined data from 2-3 experiments. In several instances, we repeated experiments more than three times to ensure reproducibility in experimental groups with high variation. In the behavioural experiments, 10-13 animals per group were used. The results are presented as mean \pm S.E., or median \pm S.D. Unpaired Student's t-test was used for all experiments except for patch clamp spike analysis in which we used Mann-Whitney U-test to determine significance between groups. P values of less than 0.05 were considered significant.

Data availability

The data that support the findings of this study are available from the corresponding author upon reasonable request.

Acknowledgments

We wish to thank Eva Lau On Chai and Prof. Xiao Qiang Yao (The Chinese University of Hong Kong) for their technical assistance with the Hecla patch clamp setup and Ekaterina Biryukova and Yana Venerina (Sechenov First Moscow State Medical University) for technical assistance for analysis of behaviour tests. The work was supported by the Lo Kwee-Seong Biomedical Research fund (The Chinese University of Hong Kong), Health and Medical Research Fund Grant, reference no. 02130636 (Hong Kong Government, Hong Kong), and the Research Grant Council-General Research Fund Grant, reference no

14113316 (Hong Kong Government, Hong Kong, and “5-100” Russian Research Excellence project.

Competing financial interests

The authors declare no competing financial interests.

References

1. Zhao, Z., Nelson, A. R., Betsholtz, C. & Zlokovic, B. V. Establishment and Dysfunction of the Blood-Brain Barrier. *Cell* **163**, 1064–1078 (2015).
2. Daneman, R., Zhou, L., Kebede, A. A. & Barres, B. A. Pericytes are required for blood–brain barrier integrity during embryogenesis. *Nature* **468**, 562–566 (2010).
3. Quaegebeur, A., Segura, I. & Carmeliet, P. Pericytes: Blood-Brain Barrier Safeguards against Neurodegeneration? *Neuron* **68**, 321–323 (2010).
4. Aspelund, A. *et al.* A dural lymphatic vascular system that drains brain interstitial fluid and macromolecules. *J. Exp. Med.* **212**, 991–9 (2015).
5. Louveau, A., Harris, T. H. & Kipnis, J. Revisiting the Mechanisms of CNS Immune Privilege. *Trends Immunol.* **36**, 569–577 (2015).
6. Ransohoff, R. M. & Engelhardt, B. The anatomical and cellular basis of immune surveillance in the central nervous system. *Nat. Rev. Immunol.* **12**, 623–635 (2012).
7. Shechter, R. & Schwartz, M. CNS sterile injury: Just another wound healing? *Trends Mol. Med.* **19**, 135–143 (2013).
8. Graeber, M. B., Li, W. & Rodriguez, M. L. Role of microglia in CNS inflammation. *FEBS Lett.* **585**, 3798–3805 (2011).
9. Pearn, M. L. *et al.* Pathophysiology Associated with Traumatic Brain Injury: Current Treatments and Potential Novel Therapeutics. *Cell. Mol. Neurobiol.* **37**, 571–585 (2017).
10. Cruz-Haces, M., Tang, J., Acosta, G., Fernandez, J. & Shi, R. Pathological correlations between traumatic brain injury and chronic neurodegenerative diseases. *Transl. Neurodegener.* **6**, 20 (2017).
11. Nelson, A. R., Sweeney, M. D., Sagare, A. P. & Zlokovic, B. V. Neurovascular dysfunction and neurodegeneration in dementia and Alzheimer’s disease. *Biochim. Biophys. Acta - Mol. Basis Dis.* **1862**, 887–900 (2016).
12. Chauhan, N. B. Chronic neurodegenerative consequences of traumatic brain injury. *Restor. Neurol. Neurosci.* **32**, 337–365 (2014).
13. Boilard, E. *et al.* Platelets Amplify Inflammation in Arthritis via Collagen-Dependent Microparticle Production. *Science (80-.)*. **327**, 580–583 (2010).
14. Thomas, M. R. & Storey, R. F. The role of platelets in inflammation. *Thromb. Haemost.* **114**, 449–458 (2015).
15. Starossom, S. C. S. C., Veremeyko, T., Dukhinova, M., Yung, A. W. Y. A. W. Y. & Ponomarev, E. D. E. D. Glatiramer acetate (Copaxone) modulates platelet activation

- and inhibits thrombin-induced calcium influx: Possible role of copaxone in targeting platelets during autoimmune neuroinflammation. *PLoS One* **9**, e96256 (2014).
16. Starossom, S. C. *et al.* Platelets play differential role during the initiation and progression of autoimmune neuroinflammation. *Circ. Res.* **117**, 779–792 (2015).
 17. Sotnikov, I. *et al.* Platelets Recognize Brain-Specific Glycolipid Structures, Respond to Neurovascular Damage and Promote Neuroinflammation. *PLoS One* **8**, e58979 (2013).
 18. Rivera, F. J., Kazanis, I., Ghevaert, C. & Aigner, L. Beyond Clotting: A Role of Platelets in CNS Repair? *Front. Cell. Neurosci.* **9**, 511 (2016).
 19. Lai, K. C. & Flaumenhaft, R. SNARE protein degradation upon platelet activation: Calpain cleaves SNAP-23. *J. Cell. Physiol.* **194**, 206–214 (2003).
 20. Barteneva, N. S. *et al.* Circulating microparticles: square the circle. *BMC Cell Biol.* **14**, 23 (2013).
 21. Mohammad-Zadeh, L. F., Moses, L. & Gwaltney-Brant, S. M. Serotonin: A review. *Journal of Veterinary Pharmacology and Therapeutics* **31**, 187–199 (2008).
 22. Gill, P., Jindal, N. L., Jagdis, A. & Vadas, P. Platelets in the immune response: Revisiting platelet-activating factor in anaphylaxis. *J. Allergy Clin. Immunol.* **135**, 1424–1432 (2015).
 23. Iwamoto, S., Kawasaki, T., Kambayashi, J., Ariyoshi, H. & Monden, M. Platelet Microparticles: A Carrier of Platelet-Activating Factor? *Biochem. Biophys. Res. Commun.* **218**, 940–944 (1996).
 24. Kawai, H. *et al.* Mice Expressing Only Monosialoganglioside GM3 Exhibit Lethal Audiogenic Seizures. *J. Biol. Chem.* **276**, 6885–6888 (2001).
 25. Wen, F.-Q., Jabbar, A. A., Patel, D. A., Kazarian, T. & Valentino, L. A. Atherosclerotic Aortic Gangliosides Enhance Integrin-Mediated Platelet Adhesion to Collagen.
 26. Ponomarev, E. D. E. D., Veremeyko, T., Barteneva, N., Krichevsky, A. M. A. M. & Weiner, H. L. H. L. H. L. MicroRNA-124 promotes microglia quiescence and suppresses EAE by deactivating macrophages via the C/EBP- α -PU.1 pathway. *Nat. Med.* **17**, 64–70 (2011).
 27. Mayo, L. *et al.* Regulation of astrocyte activation by glycolipids drives chronic CNS inflammation. *Nat. Med.* **20**, 1147–1156 (2014).
 28. Kuziemko, G. M., Stroh, M. & Stevens, R. C. Cholera toxin binding affinity and specificity for gangliosides determined by surface plasmon resonance. *Biochemistry* **35**, 6375–6384 (1996).
 29. Noguchi, M. *et al.* Unique T Cell Differentiation Markers: Gangliosides with Cholera Toxin Receptor Activity on Murine Fetal Thymocytes. *Cell. Immunol.* **156**, 402–413 (1994).
 30. Han, R., Hu, J. & Su, G. The Neuroinflammatory Response Induced by PAF Can Be Attenuated by BN52021 Administration. *Neurosci. Med.* **2**, 370–375 (2011).
 31. Kim, B. K. *et al.* Platelet-activating factor receptor knockout mice are protected from MPTP-induced dopaminergic degeneration. *Neurochem. Int.* **63**, 121–132 (2013).
 32. Tsuda, M. *et al.* Reduced pain behaviors and extracellular signal-related protein kinase activation in primary sensory neurons by peripheral tissue injury in mice lacking platelet-activating factor receptor. *J. Neurochem.* **102**, 1658–1668 (2007).
 33. Izikki, M. *et al.* Tryptophan hydroxylase 1 knockout and tryptophan hydroxylase 2 polymorphism: effects on hypoxic pulmonary hypertension in mice. *Am. J. Physiol. Lung Cell. Mol. Physiol.* **293**, L1045-52 (2007).
 34. Wuescher, L. M., Takashima, A. & Worth, R. G. A novel conditional platelet depletion

- mouse model reveals the importance of platelets in protection against staphylococcus aureus bacteremia. *J. Thromb. Haemost.* **13**, 303–313 (2015).
35. Nishihira, K. *et al.* Serotonin induces vasoconstriction of smooth muscle cell-rich neointima through 5-hydroxytryptamine_{2A} receptor in rabbit femoral arteries. *J. Thromb. Haemost.* **6**, 1207–1214 (2008).
 36. Trakhtenberg, E. F. & Goldberg, J. L. The Role of Serotonin in Axon and Dendrite Growth. *Int. Rev. Neurobiol.* **106**, 105–126 (2012).
 37. Bahrami, S. & Drabl^{??}s, F. Gene regulation in the immediate-early response process. *Adv. Biol. Regul.* **62**, 37–49 (2016).
 38. Ma, J. *et al.* Magnetic stimulation modulates structural synaptic plasticity and regulates BDNF-TrkB signal pathway in cultured hippocampal neurons. *Neurochem. Int.* **62**, 84–91 (2013).
 39. Matsuzaki, M., Honkura, N., Ellis-Davies, G. C. R. & Kasai, H. Structural basis of long-term potentiation in single dendritic spines. *Nature* **429**, 761–766 (2004).
 40. Cane, M., Maco, B., Knott, G. & Holtmaat, A. The Relationship between PSD-95 Clustering and Spine Stability In Vivo. *J. Neurosci.* **34**, 2075–2086 (2014).
 41. Castej3n, O. J., Fuller, L. & Dailey, M. E. Localization of synapsin-I and PSD-95 in developing postnatal rat cerebellar cortex. *Dev. Brain Res.* **151**, 25–32 (2004).
 42. Li, Q., Han, X. & Wang, J. Organotypic Hippocampal Slices as Models for Stroke and Traumatic Brain Injury. *Mol. Neurobiol.* **53**, 4226–4237 (2016).
 43. Chac^{??}n-Fern^{??}ndez, P. *et al.* Brain-derived neurotrophic factor in megakaryocytes. *J. Biol. Chem.* **291**, 9872–9881 (2016).
 44. Martinowich, K. & Lu, B. Interaction between BDNF and Serotonin: Role in Mood Disorders. *Neuropsychopharmacology* **33**, 73–83 (2008).
 45. Kellner, Y. *et al.* The BDNF effects on dendritic spines of mature hippocampal neurons depend on neuronal activity. *Front. Synaptic Neurosci.* **6**, 5 (2014).
 46. Nudo, R. J. Recovery after brain injury: mechanisms and principles. *Front. Hum. Neurosci.* **7**, 887 (2013).
 47. Veitinger, M., Varga, B., Guterres, S. B. & Zellner, M. Platelets, a reliable source for peripheral Alzheimer’s disease biomarkers? *Acta Neuropathol. Commun.* **2**, 65 (2014).
 48. Fragaki, K. *et al.* Refractory epilepsy and mitochondrial dysfunction due to GM3 synthase deficiency. *Eur. J. Hum. Genet.* **21**, 528–534 (2013).
 49. Wang, H. *et al.* Early growth and development impairments in patients with ganglioside GM3 synthase deficiency. *Clin. Genet.* **89**, 625–629 (2016).
 50. Lee, J. S. *et al.* GM3 synthase deficiency due to *ST3GAL5* variants in two Korean female siblings: Masquerading as Rett syndrome-like phenotype. *Am. J. Med. Genet. Part A* **170**, 2200–2205 (2016).
 51. Boccuto, L. *et al.* A mutation in a ganglioside biosynthetic enzyme, *ST3GAL5*, results in salt & pepper syndrome, a neurocutaneous disorder with altered glycolipid and glycoprotein glycosylation. *Hum. Mol. Genet.* **23**, 418–433 (2014).
 52. El Haj, M. *et al.* Apolipoprotein E (APOE) ϵ 4 and episodic memory decline in Alzheimer’s disease: A review. *Ageing Res. Rev.* **27**, 15–22 (2016).
 53. Methia, N. *et al.* ApoE Deficiency Compromises the Blood Brain Barrier Especially After Injury. *Mol. Med.* **7**, 810–815 (2001).
 54. Ponomarev, E. D., Maresz, K., Tan, Y. & Dittel, B. N. CNS-derived interleukin-4 is essential for the regulation of autoimmune inflammation and induces a state of alternative activation in microglial cells. *J. Neurosci.* **27**, 10714–10721 (2007).
 55. de las Casas-Engel, M. *et al.* Serotonin Skews Human Macrophage Polarization through HTR_{2B} and HTR₇. *J. Immunol.* **190**, 2301–2310 (2013).

56. Lai, K.-O. *et al.* TrkB phosphorylation by Cdk5 is required for activity-dependent structural plasticity and spatial memory. *Nat. Neurosci.* **15**, 1506–1515 (2012).
57. Jones, K. A. *et al.* Rapid modulation of spine morphology by the 5-HT_{2A} serotonin receptor through kalirin-7 signaling. *Proc. Natl. Acad. Sci.* **106**, 19575–19580 (2009).
58. Winnubst, J., Cheyne, J. E., Niculescu, D. & Lohmann, C. Spontaneous Activity Drives Local Synaptic Plasticity InVivo. *Neuron* **87**, 399–411 (2015).
59. Chen, Z. *et al.* Lipopolysaccharide-induced microglial activation and neuroprotection against experimental brain injury is independent of hematogenous TLR4. *J. Neurosci.* **32**, 11706–15 (2012).
60. Collins, J. M., King, A. E., Woodhouse, A., Kirkcaldie, M. T. K. & Vickers, J. C. The effect of focal brain injury on beta-amyloid plaque deposition, inflammation and synapses in the APP/PS1 mouse model of Alzheimer’s disease. *Exp. Neurol.* **267**, 219–229 (2015).
61. Choudhri, T. F., Hoh, B. L., Solomon, R. A., Connolly, E. S. & Pinsky, D. J. Use of a spectrophotometric hemoglobin assay to objectively quantify intracerebral hemorrhage in mice. *Stroke.* **28**, 2296–302 (1997).
62. Veremeyko, T., Starossom, S. C., Weiner, H. L. & Ponomarev, E. D. Detection of microRNAs in microglia by real-time PCR in normal CNS and during neuroinflammation. *J. Vis. Exp.* **65**, e4097 (2012).
63. Ponomarev, E. D., Veremeyko, T. & Barteneva, N. S. Visualization and quantitation of the expression of microRNAs and their target genes in neuroblastoma single cells using imaging cytometry. *BMC Res. Notes* **4**, 517 (2011).
64. Law, J. K. Y. *et al.* The use of SU-8 topographically guided microelectrode array in measuring extracellular field potential propagation. *Ann. Biomed. Eng.* **40**, 619–627 (2012).
65. Zheng, S. *et al.* PSD-95 is post-transcriptionally repressed during early neural development by PTBP1 and PTBP2. *Nat. Neurosci.* **15**, 381–388 (2012).

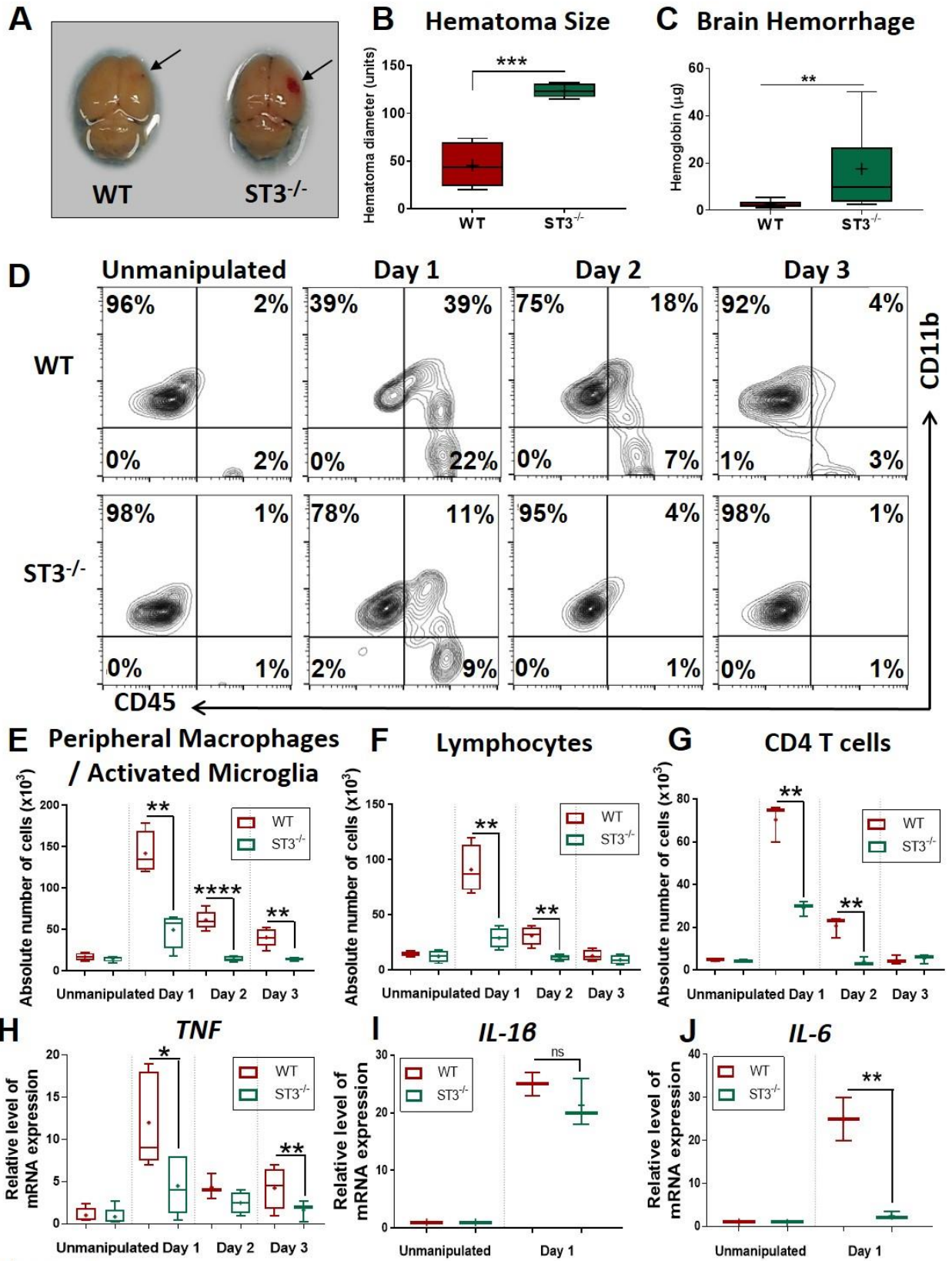


Figure 1

Figure 1. ST3^{-/-} mice exhibit a high level of intracranial hemorrhage and a low level of CNS inflammation after focal brain injury.

(A-C) Comparison of the extent of hemorrhage in WT vs. ST3^{-/-} mice after traumatic brain injury (TBI). On day 1 after TBI, animals were euthanised and perfused with PBS for brain dissection (see *Methods*). The size of the intracerebral haematoma and CNS haemoglobin concentration were measured as described in *Methods*. (A) Images of the whole brain of WT (left image) and ST3^{-/-} (right image) mice with the brain injury site marked. (B) Quantitation of haematoma size. (C) Quantitative analysis of CNS hemoglobin concentration.

In (B, C) the median ± S.D. of individual animals is shown in the box and whisker plots with mean value indicated by “+” symbol (n=6-11 of individual animals; *, p<0.05; ***, p<0.001).

(D-G) Comparison of the extent of neuroinflammation in the CNS of WT vs. ST3^{-/-} mice after TBI. Mononuclear cells were isolated from the brains of unmanipulated WT or ST3^{-/-} mice or on day 1, 2, and 3 post-TBI and expressions of CD11b and CD45 were analysed by two-colour flow cytometry as described in *Methods*. (D) Representative contour-plots with CD45 expression shown on the x-axis and CD11b on the y-axis. The percentages of cells in each quadrant are stated in each corner of the contour-plot. (E-G) Quantitative analysis of absolute numbers of peripheral macrophages/activated microglia (CD11b⁺CD45^{hi} cells), lymphocytes (CD11b⁻CD45^{hi} cells), and CD4 T cells (CD3⁺CD4⁺) is shown. (H-I) Analysis of mRNA expression for *TNF*, *IL-1B* and *IL-6* in the CNS of WT vs. ST3^{-/-} mice after TBI. mRNA was isolated from the brains of unmanipulated WT or ST3^{-/-} mice or mice with TBI and expression of mRNA for *TNF*, *IL-1B* and *IL-6* was measured by real-time RT PCR as described in *Methods*.

In (E-I), the median ± S.D. of individual animals is shown on box and whisker plot with mean value indicated by “+” symbol (n=5 of individual mice; *, p<0.05; ***, p<0.001).

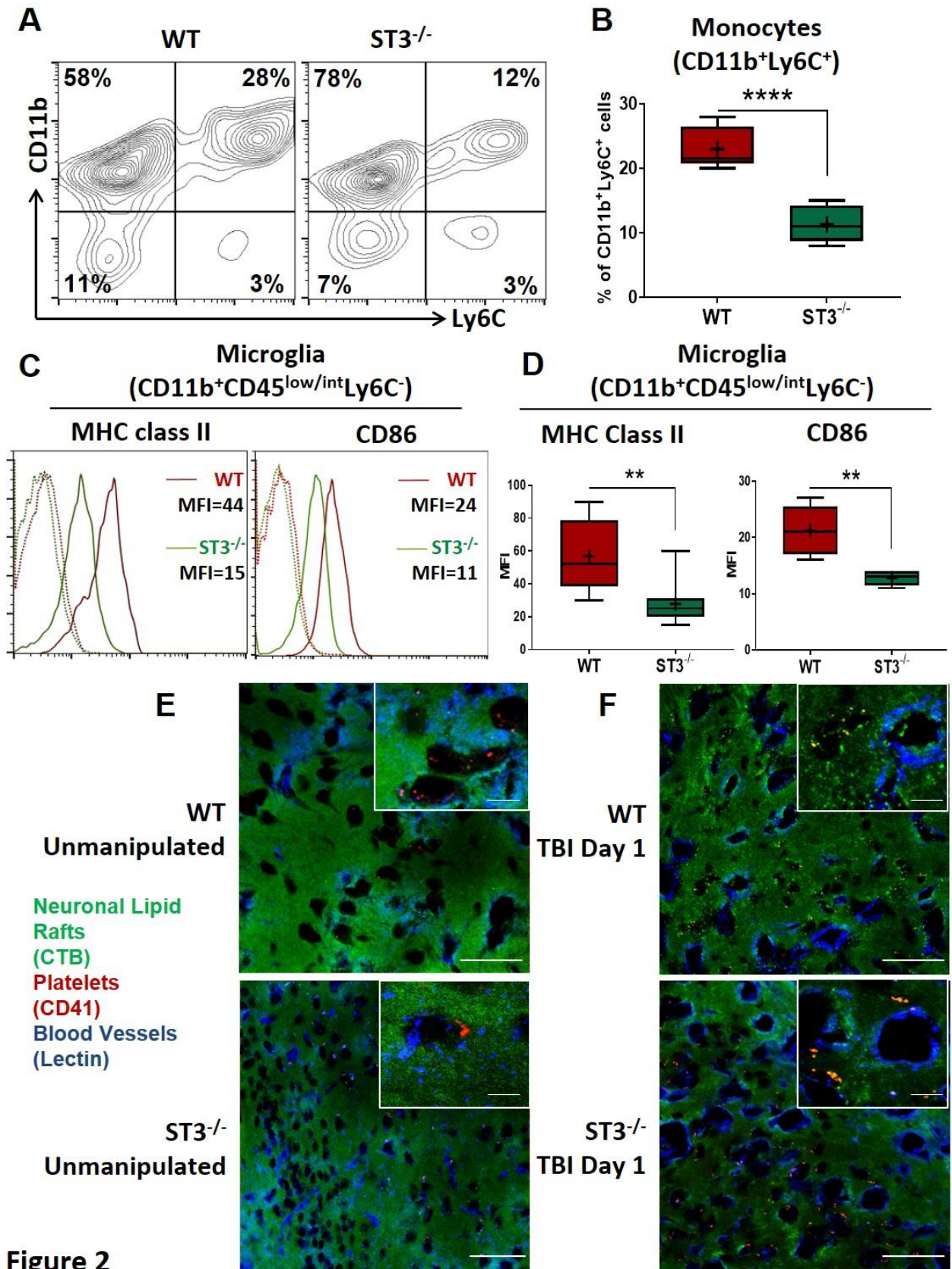


Figure 2

Figure 2. ST3^{-/-} mice have low levels of peripheral macrophage infiltration and microglia activation after traumatic brain injury.

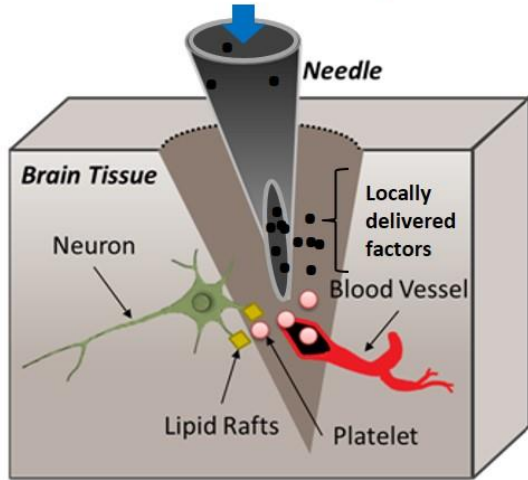
(A-E) Comparison of peripheral macrophage infiltration and microglia activation in the CNS of WT vs. ST3^{-/-} after TBI. Mononuclear cells were isolated from WT and ST3^{-/-} on day 1 post-TBI as for Fig. 1 and analyzed for expression of CD11b, Ly6C, CD45, MHC class II, and CD86 by four-color flow cytometry as described in *Methods*. (A) Representative contour-plots for expressions of Ly6C (x-axis) and CD11b (y-axis). Percentages of CNS-resident microglia (CD11b⁺Ly6C⁻ population) and peripheral monocytes/macrophages (CD11b⁺Ly6C⁺ population) are shown in the upper left and upper right quadrants, respectively. (B) Quantitative analysis of percentages of CD11b⁺Ly6C⁺ peripheral macrophages. In (B), median ± S.D. of individual animals is shown in the box and whisker plots with mean value indicated by “+” symbol (n=6 of individual mice; ****, p<0.0001).

In (C-D), CD11b⁺CD45^{low/int}Ly6C⁻ gated microglia were analyzed for the expression of activation markers MHC class II and CD86. (C) Representative histograms for the expression of MHC class II (left histogram) and CD86 (right histogram) on microglia for WT (red line) and ST3^{-/-} (green line) mice are shown. A solid line indicates staining with anti-MHC class II or anti-CD86 mAbs, and a dotted line shows staining for isotype-matched control mAbs. The mean fluorescence intensity (MFI) for MHC class II and CD86 is shown on each histogram. (D) Quantitative analyses for MFI of MHC class II and CD86 expressions on microglia.

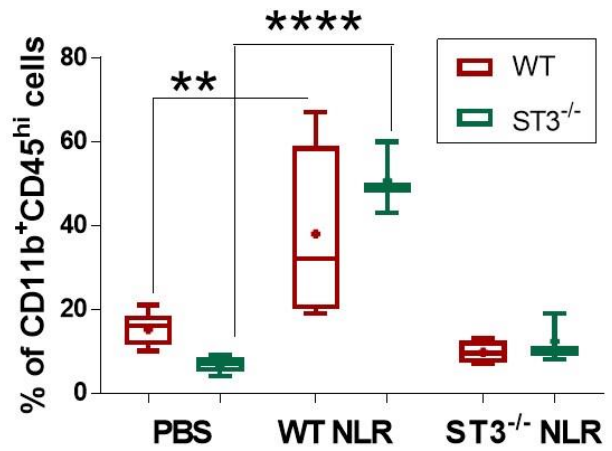
In (D), the median ± S.D. of ten individual animals is shown on box and whisker plot with mean value indicated by “+” symbol (n=10 of individual mice; *, p<0.05; **, p<0.01).

(E-F) Analysis of platelet localization in the CNS of unmanipulated WT (E) vs. ST3^{-/-} (F), or mice after TBI. Histology sections from mouse brains were prepared on d1 post-TBI and stained with anti-CD41 antibodies (platelet marker, red) and fluorescently labelled marker of neuronal lipid rafts (*Cholera Toxin B* subunit, CTB, green), and blood vessels (lectin, blue) as described in *Methods*. Representative immunofluorescence images of platelets, neuronal lipid rafts and blood vessels in the CNS of WT vs ST3^{-/-} mice at the site of injury are shown. Platelet aggregates in ST3^{-/-} mice are indicated by arrows. Bar scale represents 10 μ. The data are representative of three separate experiments.

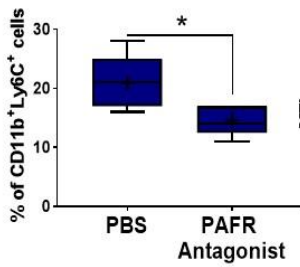
A PBS, or NLR, or PAFR antagonist, or anti-5HT serum, or 5HT



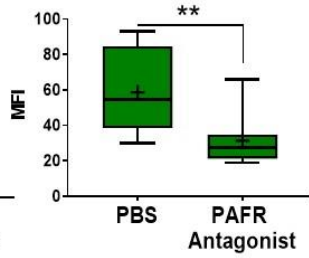
B Peripheral Macrophages / Activated Microglia



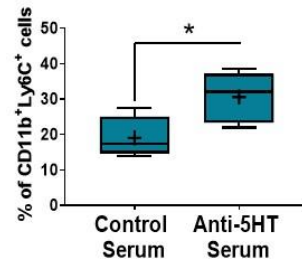
C Peripheral Macrophages



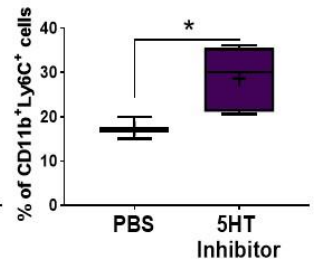
D MHC Class II on Microglia



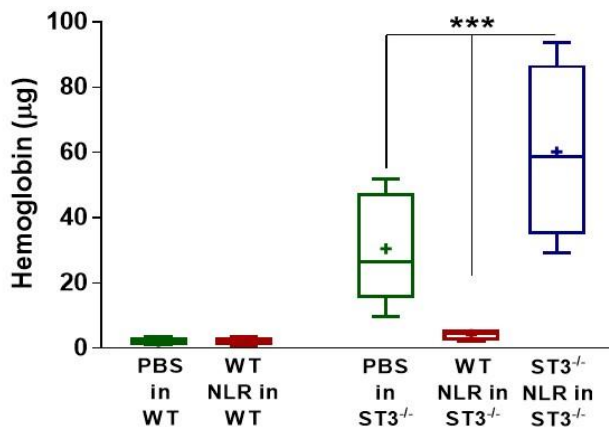
E Peripheral Macrophages



F Peripheral Macrophages



G Brain Hemorrhage



H Brain Hemorrhage

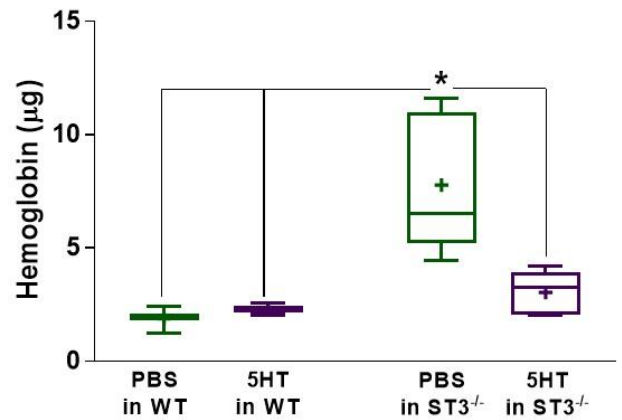


Figure 3

Figure 3. Neuronal lipid rafts from WT, but not from ST3^{-/-} mice mediate CNS inflammation and reduce hemorrhage after TBI, while platelet-derived factors PAF and 5-HT strictly control the extent of neuroinflammation and hemorrhage.

(A) Schematic diagram of experiments with local injection of PBS (as a control), neuronal lipid rafts (NLR), or PAF receptor (PAFR) antagonist, or anti-5HT serum at the site of TBI.

(B) Statistical analysis of percentages of CD11b⁺CD45^{hi} peripheral macrophages/activated microglia in the brain of WT and ST3^{-/-} mice after injection of PBS, or WT NLR, or ST3^{-/-} NLR at the site of TBI. Injection of PBS or NLR at the site of TBI was performed as described in *Methods*, mononuclear cells were isolated from the CNS on day 1 post-TBI and expressions of CD11b and CD45 were assessed by flow cytometry (see Fig.1). In (B), the median ± S.D. of individual animals is shown on box and whisker plot with mean value indicated by “+” symbol (n=3-5 of individual mice; **, p<0.01; ****, p<0.0001).

(C-D) Influence of PAF receptor (PAFR) antagonist on peripheral macrophage infiltration and microglia activation in the CNS of WT mice after TBI. Injection of PAFR antagonist WEB2086 at the site of TBI was performed as described in *Methods*, mononuclear cells were isolated from the CNS on day 1 post-TBI and expressions of CD11b, Ly6C, and MHC class II were assessed by flow cytometry (see Fig.2). (C) Statistical analysis of the percentages of CD11b⁺Ly6C⁺ peripheral macrophages and (D) MFI for MHC class II expression on CD11b⁺Ly6C⁻ microglia. In (C), the data are representative of two experiments with 5 mice per group in one experiment. In (D), the median ± S.D. of individual animals is shown on box and whisker plot with mean value indicated by “+” symbol (n=10 of individual mice; *, p<0.05; **, p<0.01).

(E-F) Influence of 5-HT inhibitors on peripheral macrophage infiltration in the CNS of WT mice after TBI. **(E)** Injection of anti-5-HT serum at the site of TBI was performed as described in *Methods*, and mononuclear cells were isolated from the CNS on day 1 post-TBI and expressions of CD11b and Ly6C were assessed by flow cytometry (see Fig.2). **(F)** Mice were systemically administrated with 5HT synthesis inhibitor p-chlorophenylalanine (PCA) for three days as described in *Methods*. At day 3 of PCA treatment, TBI was induced, and mononuclear cells were isolated from the CNS 24h later (day 1 post-TBI). The expression of CD11b and Ly6C were assessed by flow cytometry as for Fig.2. **(E)** Statistical analysis of the percentages of CD11b⁺Ly6C⁺ peripheral macrophages after anti-5-HT serum injection. **(F)** Statistical analysis of the percentages of CD11b⁺Ly6C⁺ peripheral macrophages from PCA-treated mice. **(F)**. In **(E-F)**, the median \pm S.D. of individual animals is shown with in the box and whisker plots with mean value indicated by “+” symbol (n=4-5 of individual mice; *, p<0.05).

(G-H) Analysis of extent of haemorrhage in the CNS of WT and ST3^{-/-} mice after administration of PBS, or WT neuronal lipid rafts (NLR), or ST3^{-/-} NLR, or 5-HT. Injections at the site of TBI were performed as in **(A, B)**. CNS haemoglobin concentrations were measured on d1 after TBI as for Fig. 1. **(G)** Statistical analysis of the extent of haemorrhage in the CNS of WT and ST3^{-/-} mice after administration of PBS vs. WT NLR vs. ST3^{-/-} NLR **(G)**. **(H)** Statistical analysis of extent of haemorrhage in the CNS of ST3^{-/-} mice after administration of PBS vs. 5HT. In **(G-H)**, the median \pm S.D. of individual animals is shown within in box and whisker plots with mean value indicated by “+” symbol (n=6 of individual mice; *, p<0.05; **, p<0.01).

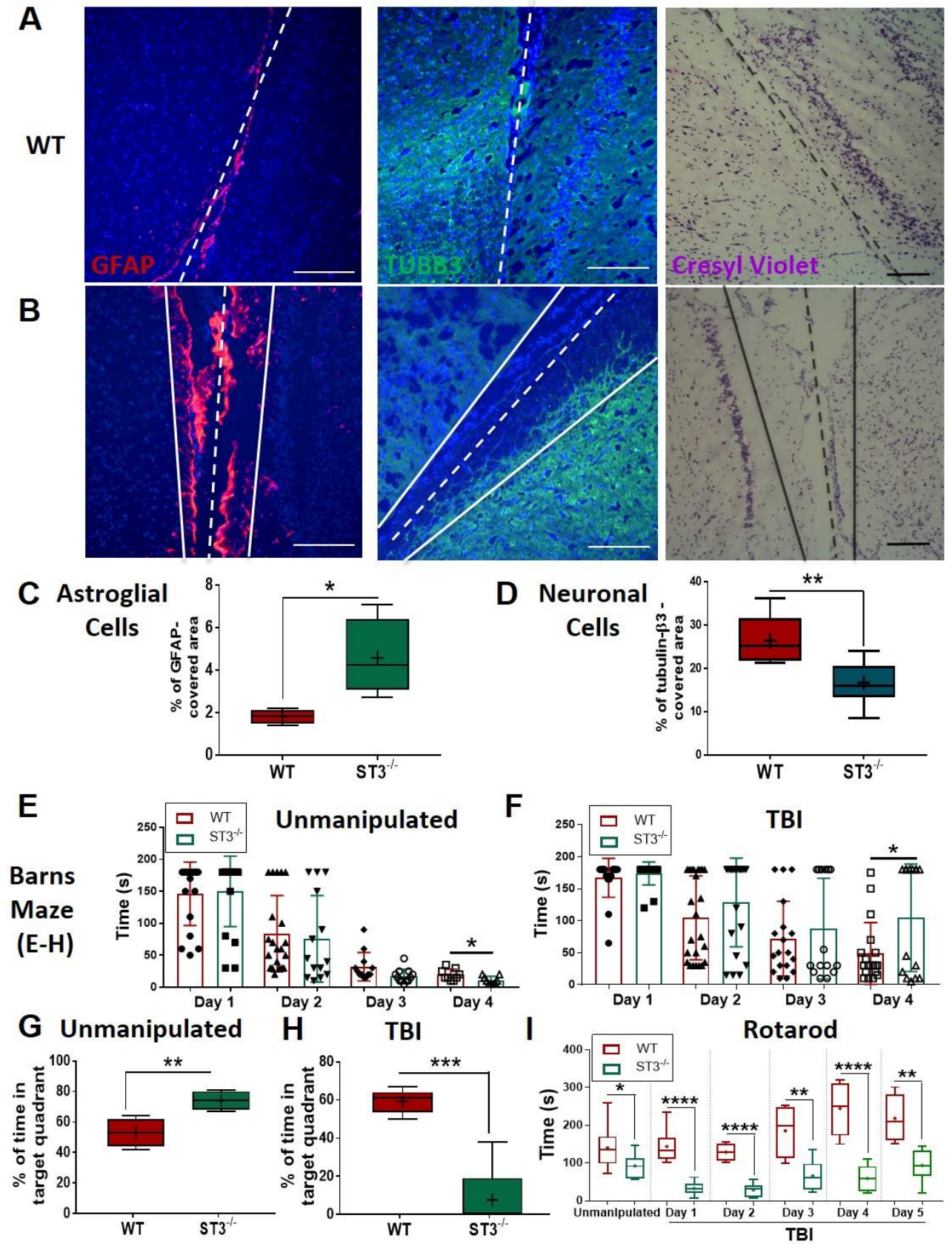


Figure 4

Figure 4. ST3^{-/-} mice have a large area of TBI-induced CNS damage with evident astroglial scar and neuronal loss after traumatic brain injury, which is associated with significant deficiencies in motor and cognitive functions.

(A-E) Brain histology from WT (left) and ST3^{-/-} (right) animals was prepared at day 7 post-TBI and tissue was stained for the astrocyte marker GFAP, neuronal cell marker β 3-tubulin and Cresyl Violet dye that detect neuronal bodies as described in *Methods*. (A) Representative image with GFAP⁺ astrocytes (red). (B) Image of the staining for neurons/neurites with anti- β 3-tubulin mAb (green). (C) Staining for neuronal bodies with Cresyl Violet. The directions of TBI are shown by punctured lines. Two solid lines show the borders of the areas of astroglial scar (GFAP⁺ red cells (A)) or loss of neurons with the absence of β 3-tubulin (green) staining (B), or nucleated neuronal cell bodies (C). (A-C) Bar scale represents 100 μ (D-E) Quantitative analysis of astrogliosis (D) and neuronal loss (E). In (D), analysis of sections from four animals with a total number of 12 section images is shown. The median \pm S.D. of overall percentage of covered area of individual animals is shown in the box and whisker plots with mean value indicated by “+” symbol (n=4 of individual mice; *, p<0.05). In (E), analysis of 1-3 sections from 5-10 animals is shown. The median \pm S.D. of overall percentage of covered area of individual animals is shown in box and whisker plots with mean value indicated by “+” symbol (n=5-10 of individual animals; **, p<0.01).

(F-I) Barnes maze (E-H) and rotarod (I) tests for unmanipulated WT and ST3^{-/-} mice (E, G, I), or on day 1, day 2, day 3, day 4 and day 5 after TBI (F, H, I). Latency time during training period (day 1 – day 4) for WT vs ST3-deficient mice is shown for Barnes maze test in (E, F) and percentage of the time in target quadrant on day 5 is shown in (G, H).

In (E-F), the median \pm S.D. of individual trials is shown (n=18-27 of individual trials; *, p<0.05). In (G-H), the median \pm S.D. of individual animals is shown (n=5-10 of individual animals; *, p<0.05; **, p<0.01; ****, p<0.0001).

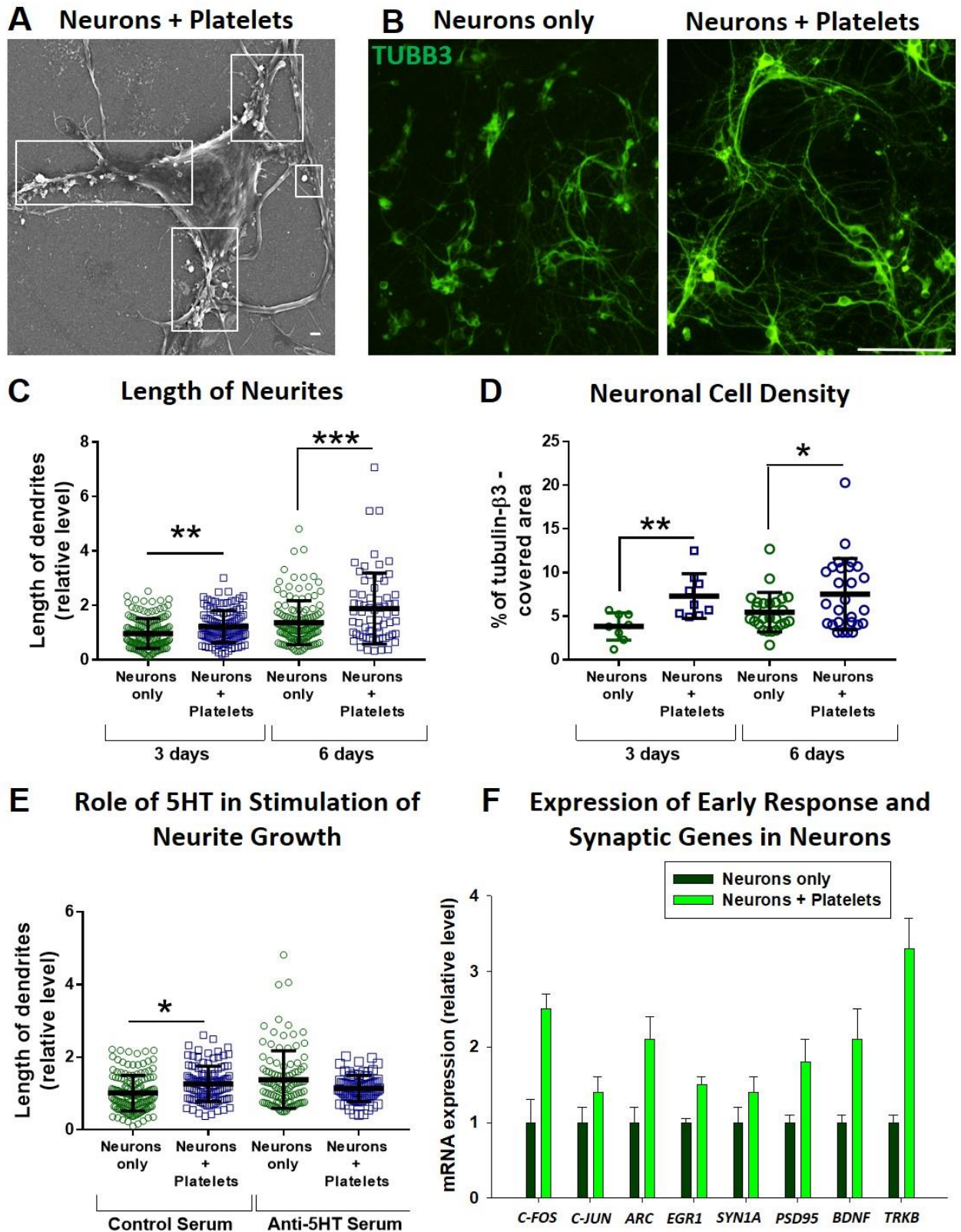


Figure 5

Figure 5. Co-incubation of platelets with cortical neurons results in active interaction of platelets with neurons, stimulation of axonal growth, and induction of a number of genes associated with neuronal activity.

Cortical neuronal cultures were prepared and co-incubated with platelets as described in *Methods*. Co-incubated platelets with neuronal cells were analysed at specific time-points by scanning electron microscopy (SEM) or immunofluorescence. For immunofluorescence, neuronal bodies and neurites were stained for β 3-tubulin as described in *Methods*.

(A) Representative SEM imaging of interaction of platelets with neuronal bodies and neurites as early as 1h after co-incubation of platelets with neurons. Platelet-neuron cell contact interactions are shown by squares. Bar scale represents 1 μ . The data is representative of three separate experiments.

(B-D) Co-incubation of platelets with neurons for 3-6 days resulted in an increase in neuronal cell density and enhanced length of neuronal process. (B) Representative images of three separate experiments for β 3-tubulin- staining (green) are shown. Bar scale represents 100 μ .

(C-D) Quantitative analysis for length of neurites (C) and neuronal cell density (D).

(E) Inhibition of platelet effect on stimulation of growth of neuronal processes by anti-serotonin serum (anti-5-HT). Platelets were co-incubated with neurons for 48 hours in the presence of anti-5-HT serum as described in *Methods* and length of neurites was assessed as in (C).

In (C, E), the analysis of total number of 50-150 processes from individual neurons from 9-12 images from 3-4 wells of culture plates is shown. Median \pm S.D. of all processes are shown (n=50-150 of individual processes; *, p<0.05; ***, p<0.001).

In (D), the analysis of total 10-30 images from 4-10 wells of culture plates is shown. Median \pm S.D. of all images are shown (n=10-30 of individual images; *, p<0.05; **, p<0.01; ***, p<0.001).

(F) Expression of mRNA for *c-Fos*, *c-Jun*, *Arc*, *Egr-1*, *Synapsin-1 α* , *PSD95*, *BDNF* and *TrkB* in neurons co-incubated with platelets. Platelets were co-incubated with neurons for 24h, after which neuronal cultures were thoroughly washed with PBS, mRNA was isolated and real-time RT PCR was performed as described in *Methods*. The data are representative of three experiments performed in triplicate; mean \pm S.D. of triplicate is shown.

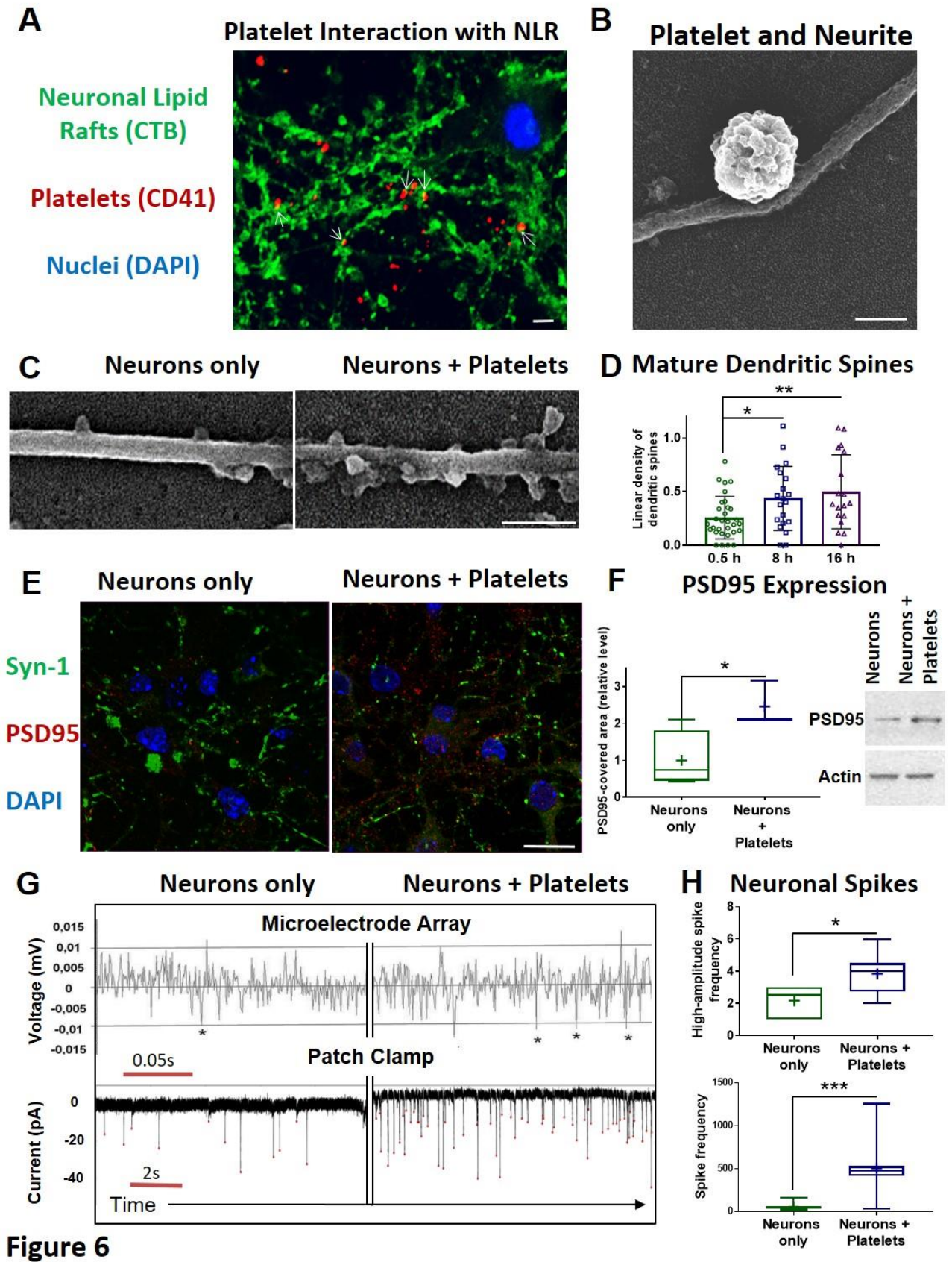


Figure 6

Figure 6. Platelets interact with lipid raft-rich neuronal processes, induce formation of PSD95-positive dendritic spines, and stimulate spontaneous electrical activity of neurons.

(A-F) Analysis of cortical neuronal cultures co-incubated with platelets with immunofluorescence (A, E) or scanning electron microscopy (B, C).

(A) Co-localisation of CD41⁺ platelets (red) with cholera toxin subunit B (CTB)-labelled neuronal lipid rafts (NLR) (green) on neuronal processes after 24h co-incubation is shown on a representative image. Arrows indicated merging signals of platelets and NLR (yellow). Bar scale represents 10 μ . The data is representative of two separate experiments.

(B) Representative SEM image showing direct contacts of platelets with neuronal processes after 1 h of **co-incubation**. Bar scale represents 1 μ . The data is representative of three separate experiments.

(C) Representative images of neuronal processes with dendritic spines for neurons cultured alone (left image) and after 8h of co-incubation with platelets (right image). Mature dendritic spines were determined as stubby or mushroom like protrusions from neuronal processes. Bar scale represents 1 μ m. The data is representative of three separate experiments.

(D) Quantitative analysis of density of mature dendritic spines on neurites for neurons incubated with platelets for 0.5, 8 and 16h. Analysis of total number of 20-30 images from 9 wells of culture plate from three separate experiments. Median \pm S.D. of quantitative analysis of all images from 9 wells is shown (n=20-30 of individual images; *, p<0.05; **, p<0.01).

(E-F) Analysis of expression of synaptic markers Synapsin-1 and PSD95 on neurons co-incubated with platelets for 24h. (E) Representative images of neurons stained for Synapsin-1 (green), PSD95 (red) and nuclei (blue). Bar scale represents 50 μ . The data is representative of three separate experiments.

(F) Analysis for the total level of PSD95 expression determined by immunofluorescence (left image) and Western blot analysis (right image). Median \pm S.D. of 3-4 culture wells is shown (*, p<0.05).

(G-H) Cortical neuronal cultures were prepared and plated on poly-L-lysine coated multielectrode array (MEA) chips or coverslips. After 24 h of co-incubation of neurons with platelets (or neurons cultured alone) the neuronal cultures were washed, placed in electrophysiology buffer and spontaneous neuronal activity was recorded using the MEA system (top figures) or patch-clamp (bottom figures) as described in *Methods*. High amplitude voltage-negative spikes with amplitude $|V|>0.01$ mV were analysed for MEA and negative current spikes above average baseline background level with $|I|>10$ pA were analysed using a patch clamp. (G) Representative recordings for spontaneous activity of neurons with MEA (top) and patch clamp (bottom). (H) Statistical analysis of neuronal spikes.

In (H, Upper), analysis of two MEA chips per experiments of three separate experiments of total number of 6 MEA chips is shown. In (H, Bottom), Analysis of 30 individual recordings from isolated cultured neurons is shown. Median \pm S.D. of quantitative analysis is shown on box and whisker plot with mean value indicated by “+” symbol (n=30 of individual recordings; *, p<0.05; ***, p<0.001).

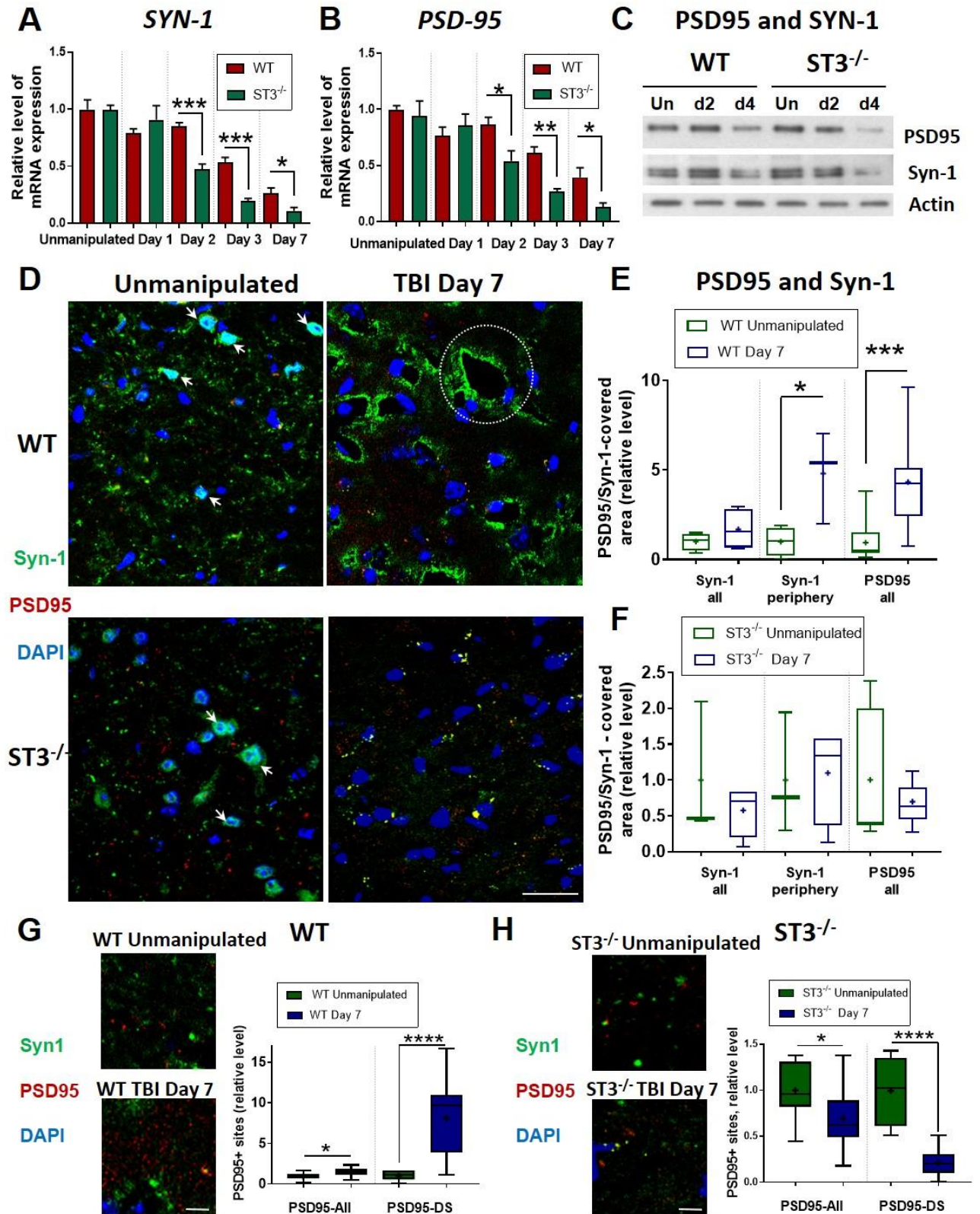


Figure 7

Figure 7. The expressions of synaptic markers Synapsin-1 and PSD95 dramatically decreased in the CNS of ST3^{-/-} mice after TBI.

(A-C) Analysis of mRNA (A, B) and protein (C) expression for Synapsin-1 α and PSD95 in WT vs. ST3^{-/-} mice in the CNS of unmanipulated mice or at day 1, 2, 3, 4 and 7 post-TBI. Induction of TBI is described in *Methods*; mRNA isolation from the brain and real-time RT PCR was performed as for Fig. 1. The mean \pm S.E. of total 4-6 individual animals shown (*, p<0.05; **, p<0.01; ***, p<0.001). Western blot analysis of representative of three separate experiment images for expression of Synapsin-1 α and PSD95 is shown in (C).

(D-H) Modulation of synaptic marker expression in the CNS of WT vs. ST3^{-/-} mice after TBI. Histology sections from mouse brains were prepared and stained for Synapsin and PSD95 as described in *Methods*. (D) Representative immunofluorescence images for expression of Synapsin-1 (*Syn1*; green), PSD95 (*PSD95*, red) and nuclei (DAPI, blue) in the CNS of unmanipulated WT (upper images) or ST3^{-/-} (lower images) mice or at the site of injury on day 7 post-TBI. Perinuclear localizations of Synapsin-1 in unmanipulated WT and ST3^{-/-} are shown by arrows. Peripheral expression of Synapsin-1 in perivascular area in WT mice on d7 post-TBI is indicated by oval. Bar scale represents 50 μ . (E-F) Quantitative analysis of PSD95, total level of Synapsin-1 (*Syn1-All*) and peripheral (not perinuclear) Synapsin-1 expressions (*Syn1-Periphery*) and PSD95 (*PSD95*) in CNS of WT (E) and ST3^{-/-} (F) mice. Synapsin-1 and PSD95 levels were quantified as immunofluorescent-covered area as for Fig. 4. (E-F) Quantitative analysis of PSD95 total level (*PSD95-All*) and the level of PSD95 on dendritic spines (*PSD95-DS*). (G-H) Quantification of relative level of expression of all PSD95-positive sites (*PSD95-All*) and a number of PSD95-positive dendritic spines that are not co-localized with Synapsin-1 (*PSD95-DS*) for CNS of WT and ST3^{-/-} mice. Representative images and statistical analysis are shown. Quantitative analysis of the total level of PSD95-expressing sites and the level of PSD95 on dendritic spines was performed as for Fig. S9.

In (E-H) median \pm S.D. of 4-20 sections of 3-4 animals is shown in box and whisker plots with mean value indicated by “+” symbol (n=4-20 of separate sections; *, p<0.05; **, p<0.01; ***, p<0.001; ****, p<0.0001).

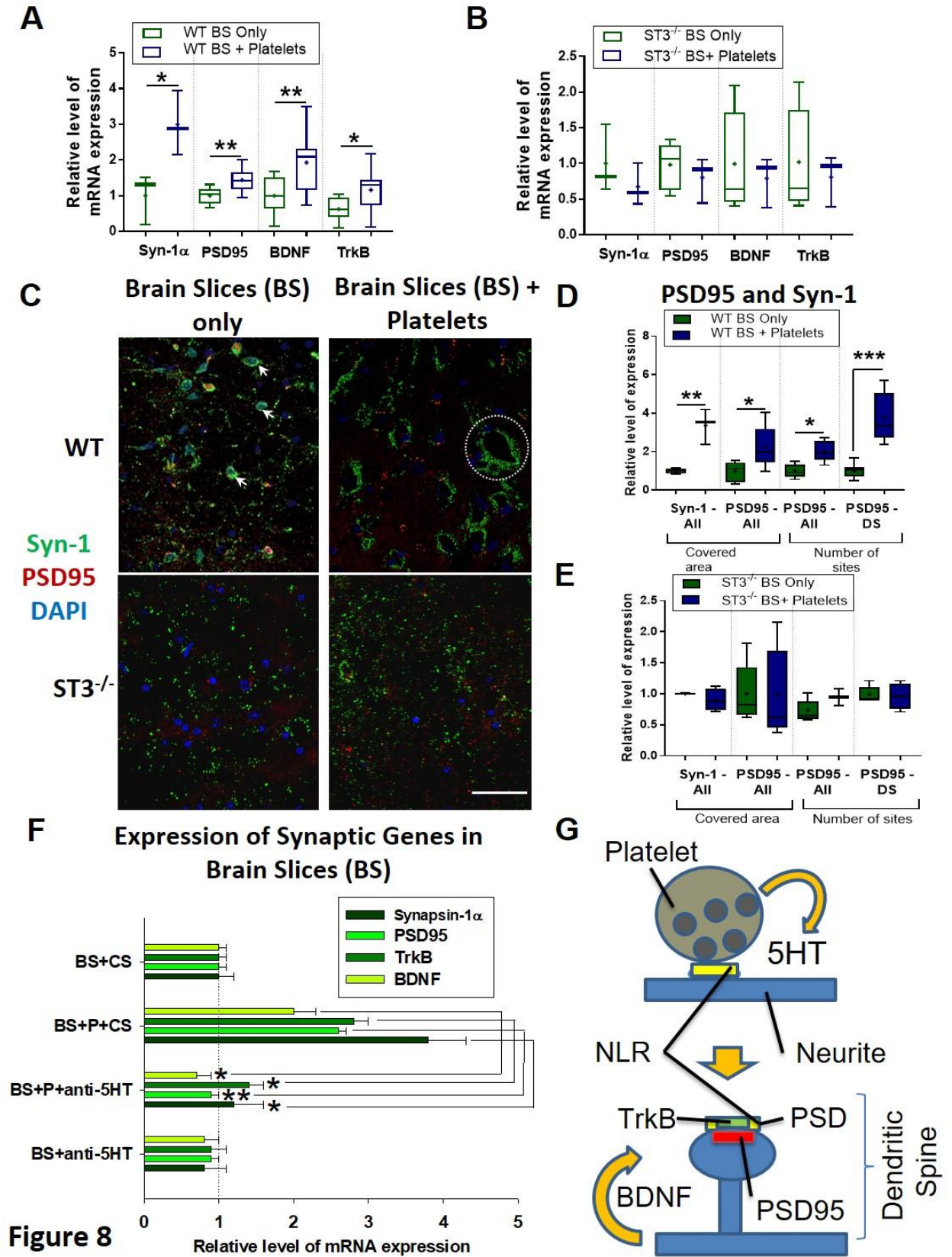


Figure 8

Figure 8. Serotonin from platelets stimulate expression of synaptic markers Synapsin-1 and PSD95 in WT but not ST3^{-/-} organotypic brain slice cultures via BDNF-TrkB pathway.

Brain slices were prepared from 3-4 week old WT or ST3^{-/-} mice as described in *Methods* and cultured alone or co-incubated with platelets for 48h. After which, brain slice cultures were washed and the expression of *Synapsin-1 α* , *PSD95*, *BDNF* and *TrkB* was evaluated on mRNA using real-time RT PCR (**A, B, F**) and the expression of Synapsin-1 and PSD95 was further investigated on a protein level using immunofluorescence microscopy (**C-E**) as described in *Methods*.

(**A-B**) Analysis of mRNA expression for *Synapsin-1 α* (*Syn1 α*), *PSD95*, *BDNF* and *TrkB* in WT (**A**) vs. ST3^{-/-} (**B**) brain slice cultures cultured alone or with platelets. Median \pm S.D. of total 3-10 separate brain slice cultures from three mice are shown in box and whisker plots with mean value indicated by “+” symbol (n=3-10 of brain slices; *, p<0.05; **, p<0.01).

(**C-E**) Analysis of expression for Synapsin-1 and PSD95 in WT vs. ST3^{-/-} brain slice cultures cultured alone or co-incubated with platelets. (**C**) Representative immunofluorescence images for the expression of Synapsin-1 (*Syn1*; green), PSD95 (*PSD95*, red) and nuclei (*DAPI*, blue) in WT or ST3^{-/-} brain slices alone or with platelets. Perinuclear localizations of Synapsin-1 in WT brain slices cultured alone are shown by using arrows. The peripheral expression of Synapsin in the perivascular area around blood vessels in WT brain slices co-incubated with platelets are indicated by an oval. The bar scale represents 100 μ (**D-E**) Quantitative analysis for levels of expression of total Synapsin (*Syn1-All*) and PSD95 (*PSD95*) for WT (**D**) and ST3^{-/-} (**E**) brain slices. Analysis of total number PSD95 expression sites (*PSD95-All*) on PSD95-positive dendritic spines (*PSD95-DS*) was performed as for Fig. 7. Median \pm S.D. of total 4-10 separate brain slice culture images from 3-4 mice are shown in box and whisker plots with mean value indicated by “+” symbol (n=4-10 brain slice cultures; *, p<0.05; ***, p<0.001).

(**F**) Analysis of mRNA expression in WT brain slices co-incubated with platelets in the presence of anti-5HT serum. WT brain slices (BS) were cultured alone or co-incubated with platelets (P) in the presence of control serum (CS) or anti-5HT serum for 48h. After which, the brain slice cultures were washed and the expression of *Synapsin-1 α* , *PSD95*, *BDNF* and *TrkB* was evaluated on mRNA using real-time RT PCR. The mean \pm S.E. of total 8 separate brain slice cultures from four mice are shown (n=8 brain slices; *, p<0.05; **, p<0.01).

(**G**) Model of stimulation of synaptic plasticity by platelets. Platelets interact with neuronal lipid rafts (NLR) of neuronal processes at the site of neuronal tissue injury, which results in platelet degranulation and secretion of 5-HT. Since mouse platelets do not produce BDNF, platelet-derived 5HT induces the expression of neuronal endogenous BDNF and their TrkB receptors that are located within NLR on post-synaptic density membranes (PSD), which in turn, result in the formation of new dendritic spines with new PSD membranes within NLR and PSD-associated PSD95.